ADVANCED MATERIALS
www.advmat.de

Lithium/Sulfide All-Solid-State Batteries using Sulfide Electrolytes

Jinghua Wu, Sufu Liu, Fudong Han, Xiayin Yao, and Chunsheng Wang**

All-solid-state lithium batteries (ASSLBs) are considered as the next generation electrochemical energy storage devices because of their high safety and energy density, simple packaging, and wide operable temperature range. The critical component in ASSLBs is the solid-state electrolyte. Among all solid-state electrolytes, the sulfide electrolytes have the highest ionic conductivity and favorable interface compatibility with sulfur-based cathodes. The ionic conductivity of sulfide electrolytes is comparable with or even higher than that of the commercial organic liquid electrolytes. However, several critical challenges for sulfide electrolytes still remain to be solved, including their narrow electrochemical stability window, the unstable interface between the electrolyte and the electrodes, as well as lithium dendrite formation in the electrolytes. Herein, the emerging sulfide electrolytes and preparation methods are reviewed. In particular, the required properties of the sulfide electrolytes, such as the electrochemical stabilities of the electrolytes and the compatible electrode/electrolyte interfaces are highlighted. The opportunities for sulfide-based ASSLBs are also discussed.

1. Introduction

Safety is a critical requirement for large-scale energy storage required in electric vehicles, airplanes, and next-generation portable electronics.[1] Compared to the currently available liquid-electrolyte lithium-ion batteries, all-solid-state lithium batteries (ASSLBs) are much safer and have high energy density because the solid electrolytes (SEs) are believed to enable to suppress the Li dendrite growth.[2] ASSLBs are believed of the prospect to break the bottleneck of liquid-electrolyte lithium-based batteries.

Dr. J. Wu, Prof. X. Yao
Ningbo Institute of Materials Technology and Engineering
Chinese Academy of Sciences
Ningbo, Zhejiang 315201, P. R. China
E-mail: yaoxy@nimte.ac.cn
Dr. J. Wu, Prof. X. Yao
Center of Materials Science and Optoelectronics Engineering
University of Chinese Academy of Sciences
Beijing 100049, P. R. China
S. Liu, Prof. F. Han, Prof. C. Wang
Department of Chemical and Biomolecular Engineering
University of Maryland
College Park, MD 20742, USA
E-mail: cswang@umd.edu
The ORCID identification number(s) for the author(s) of this article can be found under https://doi.org/10.1002/adma.202000751.

DOI: 10.1002/adma.202000751

Thirty years ago, the ASSLBs lost out in the competition with the organic-electrolyte Li-ion batteries due to the relatively low ionic conductivity of the solid electrolytes.[3–4] Significant progress has been achieved recently on improving the ionic conductivity of solid electrolytes. Kanno's group developed a sulfide solid state electrolyte that has a higher ionic electrolyte (2.5×10^{-2} S cm^{-1}) than that of the liquid ones.[5–6] Driven by the high thermal stability, high energy density, easy packaging of ASSLBS, Toyota, Sakti3, Bolloré, Solid Energy, etc.[7] are devoted to promoting the application of ASSLBs in electric vehicles and electronic devices.

Although the sulfide electrolytes offer great opportunity for ASSLBs to apply in electrochemical energy storage systems, challenges such as the narrow electrochemical stability window, poor chemical compatibility with electrodes, and poor mechanical properties should also be considered.[8–10] Herein, we focus on the sulfide electrolytes. We begin by discussing the different categories and the synthesis methods of the sulfide electrolytes. Then, the critical properties of bulk solid electrolytes (electronic conductivity, electrochemical window, air stability) and interfacial properties (chemical and electrochemical stability with electrodes) are emphasized. The efficient approaches to overcome these issues are discussed. Finally, we conclude by our perspective and recommendations on the future development of sulfide-based ASSLBs.

2. Sulfide Electrolytes

The history of solid-state ionic conductors can be dated back to 1960s, when β-alumina was used in high temperature sodium-sulfur batteries.[9] Oxide solid electrolytes were first developed, but the relatively low ionic conductivity limits its application in ASSLBs.[11] After that, Tatsumisago's group and Kanno's group explored a series of sulfide electrolytes, pushing the study of fast ion conductors to a climax and arousing a strong upsurge of interest for studying ASSLBs.[5–6,11] The high ionic conductivity of these sulfide electrolytes, which is even close to that of the organic liquid ones, make them the most promising electrolyte for ASSLBs. In addition, the sulfide electrolytes present attractive mechanical feature of plastic deformation which make it simple to prepare densely packed interface.[12–14] In general, sulfide electrolytes can be classified into two types according to the compositions:

binary and ternary sulfide electrolytes. The binary sulfide electrolytes are composed of Li_2S and P_2S_5, such as Li_3PS_4 and $Li_7P_3S_{11}$ while the ternary sulfide electrolytes consist of Li_2S, P_2S_5, MS_2 (M = Si, Ge, Sn), such as $Li_{10}GeP_2S_{12}$ (LGPS) and Li_6PS_5X (X = Cl, Br, I). According to the crystal structure, these sulfide electrolytes can be further divided into thio-LISICON (lithium superionic conductor) type, tetragonal LGPS type, and argyrodite Li_6PS_5X.

2.1. Structure of the Sulfide Electrolytes

2.1.1. Thio-LISICON

The binary $(100 - x)Li_2S$–xP_2S_5, $(100 - x)Li_2S$–$xSiS_2$ and the ternary $Li_{4-x}Ge_{1-x}P_xS_4$ ($0 < x < 1$) electrolytes, defined as thio-LISICON, are derivate from a LISICON-type γ-Li_3PO_4 solid electrolyte by replacing oxygen with sulfur. The thio-LISICON electrolytes normally possess higher Li^+ conductivity than the oxide counterparts because the electronegativity of S is lower than O, which results in the smaller Li^+ binding energy and the larger ionic migration channel thus facilitate the movement of Li^+.[5] As a result, thio-LISICON have ionic conductivities of 10^{-3}–10^{-4} S cm^{-1} at room temperature, much higher than that of most oxide electrolytes.[5–6]

Generally, the ionic conductivity of glass is one or two orders of magnitude higher than that of the crystalline one at the same composition.[15] The absence of crystallinity is the main reason for eliminating grain boundary resistance. The open structures and large free volume of the amorphous glass enable it with the higher ionic conductivity than crystalline.[16] In order to enhance ionic conductivity of binary sulfide electrolyte, Tatsumisago's group systematically investigated conductive properties of Li_2S–P_2S_5 systems by controlling the compositions and heat treatment temperatures of the mechanically milled $(100 - x)Li_2S$-xP_2S_5 glasses.[17–20] For all these electrolytes, the glass–ceramic types always exhibit higher ionic conductivity than the glass or crystalline materials. The enhancement of ionic conductivity is mainly due to the precipitation of metastable thio-LISICON analogs. For example, the ionic conductivity of $80Li_2S$–$20P_2S_5$ and $75Li_2S$–$25P_2S_5$ glass–ceramic increased to 7.2×10^{-4} and 2.8×10^{-4} S cm^{-1}, while the ionic conductivity of the as prepared glasses were only 1.7×10^{-4} and 1.8×10^{-4} S cm^{-1}, respectively.[17] X-ray diffraction (XRD) pattern showed that the thio-LISICON II analog and thio-LISICON III analog were precipitated in $80Li_2S$–$20P_2S_5$ and $75Li_2S$–$25P_2S_5$ glasses. Similarly, $70Li_2S$–$30P_2S_5$ glass–ceramic showed an enhanced ionic conductivity as high as 3.2×10^{-3} S cm^{-1} after annealing at 360 °C, which can also be attributed to a new crystal as a metastable phase.[18,20] The structure of new phase, $Li_7P_3S_{11}$, was determined using synchroton XRD as shown in **Figure 1**a. The crystalline phase belongs to triclinic system of space group $P\bar{1}$. Specifically, $P_2S_7^{4-}$ ditetrahedra and PS_4^{3-} tetrahedra are contained in it with lithium ions located between them, which is similar to that of the Ag-ion conductor $Ag_7P_3S_{11}$ (Figure 1b).[21]

The $Li_7P_3S_{11}$ further modified by the doping, such as $Li_7P_{2.9}Mn_{0.1}S_{10.7}I_{0.3}$, exhibited an ionic conductivity of 5.6×10^{-3} S cm^{-1}.[22] The Li_3PS_4 glass–ceramic has a relatively low conductivity of nearly 1.6×10^{-4} S cm^{-1} compared with $80Li_2S$–$20P_2S_5$ and $Li_7P_3S_{11}$.[23] However, it delivered better chemical stability against Li metal than $Li_7P_3S_{11}$. The original PS_4^{3-} group of Li_3PS_4 has good chemical stability against hydrolysis which reduces the generation of H_2S and the large structural changes when it is exposed in air.[24] The structure of γ-Li_3PS_4 and β-Li_3PS_4 are shown in Figure 1c,d. Bulk Li_3PS_4 with a γ-phase exhibits a relatively low ionic conductivity of 3×10^{-7} S cm^{-1}, but it will convert into a high conducting β-Li_3PS_4 after heating, which shows an abrupt increase of ionic conductivity.[23]

Jinghua Wu is an associate professor at Ningbo Institute of Materials Technology and Engineering, Chinese Academy of Science (NIMTE, CAS). He received his Bachelor of Science (BS) degree from Shandong University, China in 2006 and his Ph.D. degree from NIMTE in 2012. After postdoctoral research at the National Institute for Materials Science (NIMS, Japan) and Soochow University, he joined NIMTE as an associate professor in 2018. His research interests focus on sulfide-electrolyte-based solid-state batteries and solid-state lithium-sulfide batteries.

Xiayin Yao is a professor at Ningbo Institute of Materials Technology and Engineering, Chinese Academy of Sciences (NIMTE, CAS). He received his Ph.D from Institute of Solid State Physics and NIMTE, CAS in 2009. After that, he joined NIMTE and has worked there until now. He worked as a research fellow or visiting scholar in Hanyang University, South Korea (2012–2013), Nanyang Technological University, Singapore (2013–2014) and University of Maryland, College Park USA (2018–2019). His major interests include all-solid-state lithium/sodium batteries.

Chunsheng Wang is Robert Franklin and Frances Riggs Wright Distinguished Chair Professor in the Department of Chemical & Biomolecular Engineering & Chemistry and Biochemistry at the University of Maryland. He is UMD Director of The UMD-ARL Center for Research in Extreme Batteries. His research focuses on rechargeable batteries.

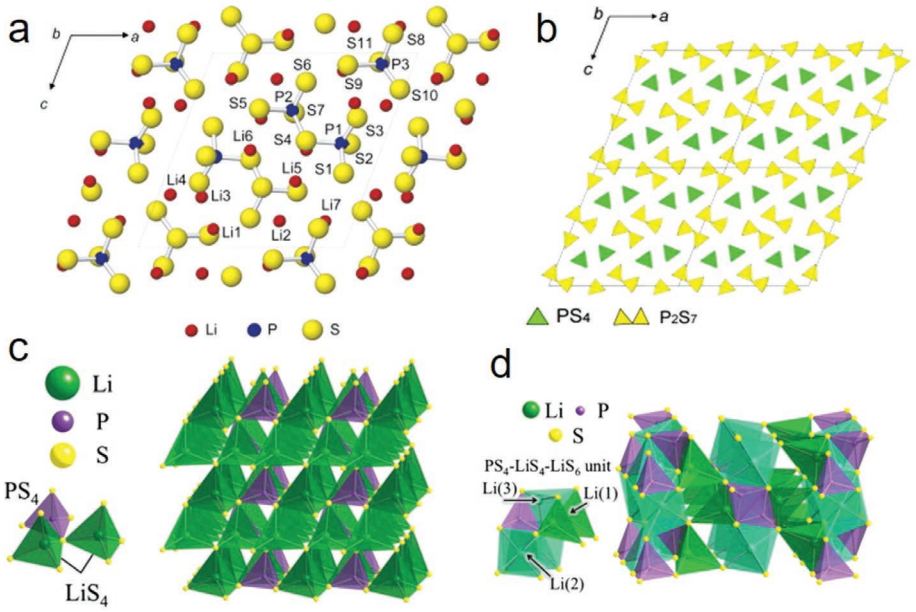

Figure 1. a) Structure of $Li_7P_3S_{11}$ viewed along the [010] direction. b) Structure of $Ag_7P_3S_{11}$ viewed along the [010] direction. a,b) Reproduced with permission.[21] Copyright 2007, Elsevier. c) Structure of γ-Li_3PS_4. d) Structure of β-Li_3PS_4. c,d) Reproduced with permission.[25] Copyright 2011, Elsevier.

Besides the composition and the crystal structure, the packing density of the electrolyte can also affect the ionic conductiviy. Seino et al. found that the ionic conductivity of $Li_7P_3S_{11}$ can increase to 1.7×10^{-2} S cm^{-1} after densification at 280 °C, which is even higher than that of organic liquid electrolytes. The high ionic conductivity is attributed to its low porosity as well as a low grain boundary resistance.[11] As shown in **Figure 2**a,b, the grain boundary of the sulfide electrolytes normally has less impact on its ionic conductivity if the ionic conductivity of the bulk electrolytes is low. However, the grain boundary can significantly affect ionic conduction when the ionic conductivity of the bulk electrolytes is high such as in the unified glass–ceramic Li_2S–P_2S_5 materials.

To further optimize the $(100 - x)Li_2S$–xP_2S_5 system, the other ingredient such as GeS_2, SiS_2, SnS_2, or Al_2S_3 were added to the $(100 - x)Li_2S$-xP_2S_5 system to form ternary Li_2S–M_xS_y–P_2S_5. A series of electrolytes like Li_2S–GeS_2 (Li_2GeS_3), Li_4GeS_4, Li_2S–GeS_2–ZnS system (Li_2ZnGeS_4), $Li_{4-2x}Zn_xGeS_4$, $LiGaS_2$, Li_5GaS_4, and Li_2S–GeS_2–Ga_2S_3 system were synthesized by Kanno's group.[26] Among them, Li_2S–GeS_2–Ga_2S_3 exhibited the highest ionic conductivity of 6.5×10^{-5} S cm^{-1} and a wide electrochemical stability of 5V versus Li/Li$^+$.[26] Kanno's group further obtained the $Li_{4-x}Ge_{1-x}P_xS_4$ ($0 < x < 1$) structures by partial doping P^{5+} at Ge^{4+} sites. According to the composition regions, there are three types of $Li_{4-x}Ge_{1-x}P_xS_4$ ($0 < x < 1$): type I ($0 < x < 0.6$), type II ($0.6 < x < 0.8$) and type III ($0.8 < x < 1$). The electrolytes in region II exhibited highest ionic conductivity than that of other two regions.[27] The ionic conductivity of $Li_{3.25}P_{0.75}Ge_{0.25}S_4$ reached the maximum of 2.2×10^{-3} S cm^{-1}.[27] Shinya et al. evaluated the coefficient and activation energy of $Li_{4-x}Ge_{1-x}P_xS_4$ by quantum molecular dynamics and found that the diffusion process was triggered by the excess lithium atoms and lithium vacancies through lithium interstitial or vacancy mechanism.[28]

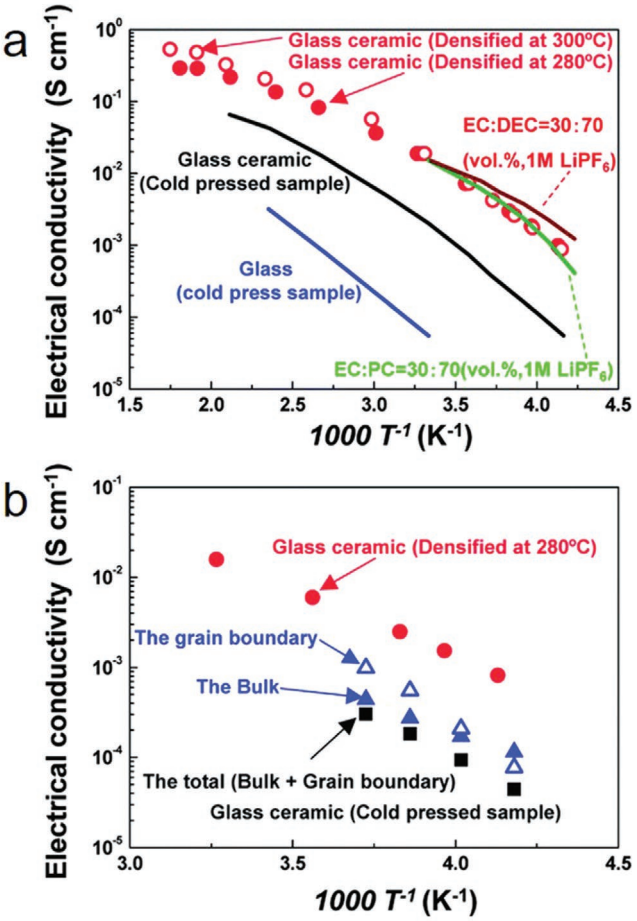

Figure 2. a) Arrhenius plots of $Li_7P_3S_{11}$. b) The bulk and grain boundary resistances of the glass–ceramic material. a,b) Reproduced with permission.[11] Copyright 2014, Royal Society of Chemistry.

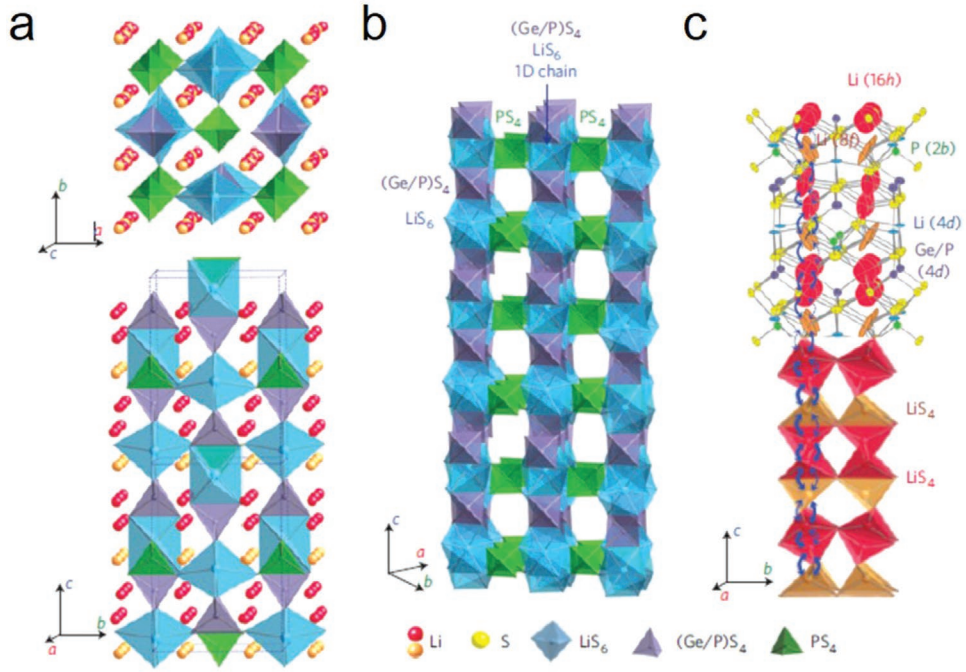

Figure 3. Crystal structure of $Li_{10}GeP_2S_{12}$. Reproduced with permission.[5] Copyright 2011, Springer Nature.

2.1.2. $Li_{11-x}M_{2-x}P_{1+x}S_{12}$ (M = Ge, Sn, Si)

In 2011, Kamaya et al. reported an new ternary $Li_{10}GeP_2S_{12}$ electrolyte with a new 3D framework structure.[5] Although the $Li_{10}GeP_2S_{12}$ has the same element compositions with thio-LISICON of $Li_{4-x}Ge_{1-x}P_xS_4$, this new electrolyte shows different structure consisting of $(Ge_{0.5}P_{0.5})S_4$ tetrahedrons, PS_4 tetrahedrons, LiS_4 tetrahedrons, and LiS_6 octahedrons. **Figure 3** shows the crystal structure of $Li_{10}GeP_2S_{12}$. A 1D chain along c axis consists of $(Ge_{0.5}P_{0.5})S_4$ tetrahedra and LiS_6 octahedra by sharing a common edge. These 1D chains are interconnected by PS_4 tetrahedra by sharing a common corner with LiS_6 to form a 3D framework.

$Li_{10}GeP_2S_{12}$ is the first solid electrolyte that exhibits an extremely high ionic conductivity of 1.2×10^{-2} S cm^{-1}.[5] Kuhn et al. used multitude techniques to study the Li ion dynamics of $Li_{10}GeP_2S_{12}$. They found that the high ionic conductivity of $Li_{10}GeP_2S_{12}$ can be attributed to the isotropic Li ions hopping in the bulk lattice where $E_a \approx 0.22$eV.[29] The development of $Li_{10}GeP_2S_{12}$ is a significant step toward realization of ASSLB. However, the expensive and rare germanium and the narrow electrochemical stability window limit its application for high power and energy densities. To address these challenges, LGPS-family described as $Li_{11-x}M_{2-x}P_{1+x}S_{12}$ (LMPS, M = Si, Ge, Sn) were comprehensively investigated. Ong et al., Bron et al. and Kuhn et al. predicted the decreasing activation energies of the lithium-ion diffusion process and increasing ionic conductivity in the series M = Sn → Ge → Si in $Li_{11-x}M_{2-x}P_{1+x}S_{12}$ system by theoretical studies.[30–32] The substitute of Ge by Si/Sn will reduce the cost of these electrolytes greatly. However, the ionic conductivity of $Li_{10}SiP_2S_{12}$ is lower than that of $Li_{10}GeP_2S_{12}$.[33–36] Kanno et al. later synthesized new members to the LGPS family: $Li_{10.35}Si_{1.35}P_{1.65}S_{12}$ (2×10^{-2} S cm^{-1}),[37] and a chlorine-containing compound $Li_{9.54}Si_{1.74}P_{1.44}S_{11.7}Cl_{0.3}$,[6] which exhibits the highest ionic conductivity reported to date (2.5×10^{-2} S cm^{-1}). The analogical $Li_{9.54}Si_{1.74}P_{1.44}S_{11.7}I_{0.3}$ recent was proved to not only have an ionic conductivity as high as 1.35×10^{-3} S cm^{-1} but also possess a electrochemical window up to 9 V versus Li/Li$^+$.[38] Therefore, the LGPS-type electrolytes are becoming one of the most attractive solid electrolytes. To further enhance the electrochemical stability window, $Li_{9.42}Si_{1.02}P_{2.1}S_{9.96}O_{2.04}$ was synthesized by the introduction of oxygen into the LGPS-type structure which exhibited an ionic conductivity of 3.2×10^{-4} S cm^{-1}. Although the ionic conductivity of $Li_{9.42}Si_{1.02}P_{2.1}S_{9.96}O_{2.04}$ was lower than that of $Li_{10}GeP_2S_{12}$, the all-solid-state cell with a lithium metal anode and $Li_{9.42}Si_{1.02}P_{2.1}S_{9.96}O_{2.04}$ as the electrolyte present an excellent electrochemical stability with reversibility of nearly 100%.[39]

2.1.3. Li_6PS_5X (X = Cl, Br, I)

The mineral argyrodite (Ag_8GeS_6) is a group of solids that have a high ionic conductivity and mobility of their Ag$^+$ ions.[40] Triggered by the great interesting in the mobility of Li$^+$ ion in solid, Li_6PS_5X (X: Cl, Br, I) systems were explored to worked as the solid electrolytes. Take Li_6PS_5I as sample (**Figure 4**), the cell is composed by 136 tetrahedral formed by the S (S1) atoms. The P atoms of Li_6PS_5I are filled four of the tetrahedral holes. The four octants of the cell are occupied by the single S^{2-} ions (S2). I ions are found at the corners and the face of the cell. Li ions with disordered mode take part of the 132 tetrahedral holes which are formed by S2 and I.[41]

The Li_6PS_5I demonstrated a relatively low conductivity of 4×10^{-7} S cm^{-1}.[42] The ordering of the larger I$^-$ compared to the disorder of Cl$^-$ or Br$^-$ ions was believed to invoke the low

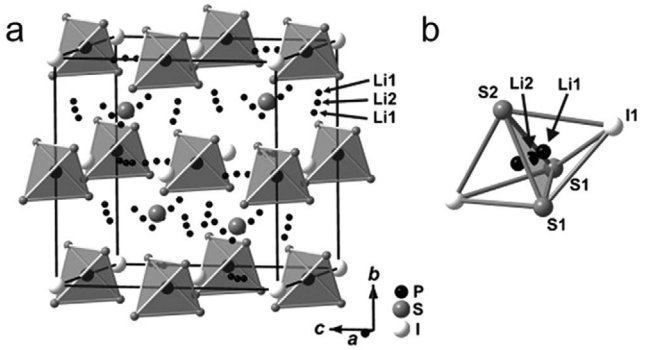

Figure 4. a) Crystal structure of Li_6PS_5I. b) A face-sharing S_3I_2 double tetrahedron containing Li1. a,b) Reproduced with permission.[41] Copyright 2008, Wiley-VCH.

conductivity. Sylvain et al. synthesized a series of Li_6PS_5X (X: Cl, Br, I). Among them, the Li_6PS_5Cl presented the attractive ionic conductivity of 1.33×10^{-3} S cm^{-1}.[43] Zhou et al. report a solution-engineered to synthesized a series of $Li_{6-\gamma}PS_{5-\gamma}Cl_{1+\gamma}$ (γ = 0–0.5) and obtained a high ionic conductivities of 3.9×10^{-3} S cm^{-1} and negligible electronic conductivities.[44] Kraft et al. studied the effect of lattice polarizability on the ionic conductivity of the Li_6PS_5X by adjusting the fractional occupancy of the halide anions. They found that the stiffness of the lattice for Li_6PS_5X is an important factor to determine the ionic conductivity.[45] Very recently, Parvin et al. reported a Cl-rich $Li_{5.5}PS_{4.5}Cl_{1.5}$ argyrodites, which exhibited a conductivity of 9.4×10^{-3} S cm^{-1} after cold-pressing and 12×10^{-3} S cm^{-1} after sintered. The substitution of S^{2-} with Cl^- helps to increase site disorder and concentration of lithium vacancy, which are considered important for enhancing Li^+ diffusivity.[46] Craft further doped Ge into Li_6PS_5I to form $Li_{6+x}P_{1-x}Ge_xS_5I$, achieving an ionic conductivity up to 5.4×10^{-3} S cm^{-1} in cold-pressed state and 1.8×10^{-2} S cm^{-1} after sintering.[47] In these argyrodites, the disorder of anion site is considered to lower the activated barrier of Li-ion transfer thus is beneficial for obtaining high Li^+ conductivity.

Up to now, Li_6PS_5Cl is consequently a promising candidate among all the argyrodites electrolytes due to its high ionic conductivity.[48–50] The conductivities of these materials are slightly lower than that of $Li_{10}GeP_2S_{12}$. However, the much cheaper precursors make this material more attractive for the practical application in ASSLB. Besides the ionic conductivities, a wide electrochemical window (7 V vs Li/Li$^+$) is also reported for Li_6PS_5Cl.[43]

2.2. Synthesis Method

Several methods have been used for synthesis of the sulfide electrolytes. The most common methods are mechanical ball-milling, solid-state method, and liquid phase synthesis.

2.2.1. Room-Temperature Mechanical Ball-Milling

Mechanical ball-milling is the commonly used method to prepare sulfide electrolytes because it is relatively lower cost and simple operation. Most $(100 - x)Li_2S$–xP_2S_5 solid electrolytes are prepared by mechanical milling and annealing.[19,21] Phuc et al. prepared the Li_3PS_4 by a liquid-phase shaking, however, the ionic conductivity is only 6.4×10^{-6} S cm^{-1}, which is much lower than that prepared by ball milling.[51] Tatsumisago's group compared the effect of milling period for the ionic conductivity of Li_2S–SiS_2 system. As the milling time increased, the grains drastically decreased and homogeneous fine particles were obtained. The conductivity of the sample increased from 10^{-8} S cm^{-1} at 100 °C to higher than 10^{-4} cm^{-1}.[52] A series of $(100 - x)$ Li_2S–xP_2S_5 electrolytes were synthesized using the ball-milling method, such as $70Li_2S$–$30P_2S_5$ (8.6 mS cm^{-1}),[53] $77.5Li_2S$–$22.5P_2S_5$ (1 mS cm^{-1}),[54] 75 Li_2S–$25P_2S_5$(0.5 mS cm^{-1}),[55] and $80Li_2S$–$20P_2S_5$ (0.72 mS cm^{-1})[17,40]. By combining the mechanical milling with hot pressing, the ionic conductivity of $Li_7P_3S_{11}$ was further increased from 3.2×10^{-3} to 7.3×10^{-3} S cm^{-1}.[53,56] A $Li_7P_3S_{11}$-analog such as $Li_7P_{2.9}Mn_{0.1}S_{10.7}I_{0.3}$ was also prepared by a high-energy ball milling method.[22] Kanno's group synthesized the $Li_{9.54}Si_{1.74}P_{1.44}S_{11.7}Cl_{0.3}$ with the super high conductivity of 25 mS cm^{-1} by the high ball milling for 120 h. The Li_6PS_5X (X = Cl, Br, I) argyrodites were synthesized by high-energy ball milling presented a high conductivity between 2 and 7×10^{-4} S cm^{-1}. Further optimizing the milling time, the ionic conductivity of Li_6PS_5Cl can reach to 1.33×10^{-3} S cm^{-1}.[43]

The ball milling techniques have been proven suitable for preparing amorphous materials at room temperature. It is widely believed that fine powders can achieve high ionic conductivities as well as intimate contact with electrode materials for ASSLB assembly. For $(100 - x)$ Li_2S–xP_2S_5 systems, the amorphous materials of glass–ceramic electrolyte can be obtained by high-energy milling. The high Li^+ conductivity of $(100 - x)$ Li_2S–xP_2S_5 can be obtained in the glass–ceramic because the Li^+ concentration in the mixture exceeds the glass formation limit.[52]

2.2.2. High-Temperature Solid-State Reaction Method

The melt-quenching and high-temperature process is proved valid to enhance the ionic conductivity of the electrolytes. For melt-quenching method, the chemicals were sealed and heated at the melting point. After that, the sample was rapidly quenched or slowly cooled to room temperature. Li_2S–P_2S_5 glass–ceramic which delivered the conductivity of 1.7×10^{-2} S cm^{-1} can be obtained by combining this melt-quench and cold-press method.[11] γ-Li_3PS_4 and β-Li_3PS_4 were synthesized by heating to a fixed reaction temperature and then slow cooling to room temperature.[25] The most attractive $Li_{10}GeP_2S_{12}$, was also synthesized by reacting stoichiometric precursors (LiS, GeS_2, and P_2S_5) at 550 °C in an evacuated quartz tube.[5] LGPS-analog, $Li_{9.42}Si_{1.02}P_{2.1}S_{9.96}O_{2.04}$ was synthesized by quenching from 1273 K in the Li_2S–P_2S_5–SiO_2 system.[39] Another series of LGPS-based electrolytes with the general formula $Li_{11-x}M_{2-x}P_{1+x}S_{12}$ with M = Ge, Sn, Si were prepared by high-pressure synthesis at 723 K with pressures in the range 3–5 GPa.[32] Li_6PS_5Cl prepared by annealing at 550 °C for 5h has a high ionic conductivity of 1.18×10^{-3} S cm^{-1}.[48] The conductivity was further enhanced to 3.15×10^{-3} S cm^{-1} by a rapid solid-state route,[57] A value of 5×10^{-3} S cm^{-1} for Li_6PS_5Cl was recently obtained through annealing and pressed at high pressure.[58]

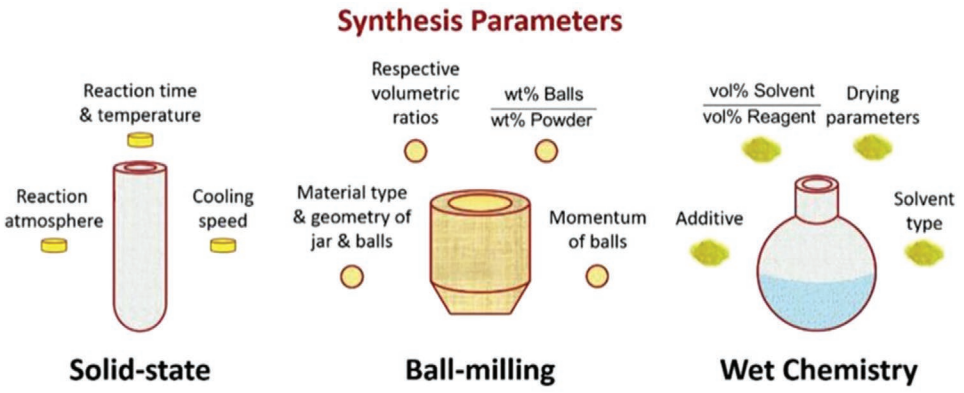

Figure 5. Parameters of the ball-milling, solid-state route and liquid-phase preparation. Reproduced with permission.[68] Copyright 2018, Elsevier.

2.2.3. Liquid-Phase Synthesis

Considering the interfacial compatibility between the solid electrolyte and solid electrode, the controllable liquid-phase synthesis of the sulfide electrolytes is more desirable for compositing with the electrode. Ito et al. synthesized crystalline $Li_7P_3S_{11}$ by a liquid-phase reaction of Li_2S and P_2S_5 in 1,2-dimethoxyethane (DME) solvent, and the ionic conductivity is 2.7×10^{-4} S cm^{-1}.[59] As the most promising solid electrolytes, $Li_7P_3S_{11}$ glass–ceramic electrolyte were further synthesized use different solvent to avoid the impurity introduced by 1,2-dimethoxyethane.[60–61] Yao et al. synthesized $Li_7P_3S_{11}$ glass–ceramic electrolyte with the ionic conductivity of 1.5×10^{-3} S cm^{-1} by a solution of acetonitrile (ACN).[62] Then Wang et al.[63] found the two-step reactions of crystalline $Li_7P_3S_{11}$ in ACN as follows:

$$\begin{aligned} &x\mathrm{Li_2S} + (100-x)\,\mathrm{P_2S_5} + \mathrm{ACN} \rightarrow 2(x-50) \\ &\quad \mathrm{Li_3PS_4} \times \mathrm{ACN(p)} + 2(75-x)\,\mathrm{Li_2S} \times \mathrm{P_2S_5} \end{aligned} \tag{1}$$

The $Li_3PS_4 \cdot ACN$ precipitates and the $Li_2S \cdot P_2S_5$ glass first generated from the supernatant forms. After ACN evaporation, the amorphous $Li_2S \cdot P_2S_5$ appears to be covered on the precipitate particles. A conductivity of 0.87×10^{-3} S cm^{-1} of $Li_7P_3S_{11}$ was obtained by the liquid method which is lower than that synthesized using solid-state method.[63] Liu et al. synthesized β-Li_3PS_4 in tetrahydrofuran (THF), which delivered an anomalous room-temperature ionic conductivity of 1.6×10^{-4} S cm^{-1}.[23] Teragawa et al. synthesized the Li_3PS_4 by a liquid-phase reaction. The Li_2S and P_2S_5 were used as precursor and the *N*-methylformamide and *n*-hexane as media. This approach leads to a polycrystalline Li_3PS_4 with an ionic conductivity of 2.3×10^{-6} S cm^{-1}.[64]

Solution-based Li_6PS_5X synthesis routes typically lowered the ionic conductivity to 10^{-5}–10^{-4} S cm^{-1} owing to phase impurities.[65] Li_6PS_5Cl was synthesized in ethanol solution, which exhibited an ionic conductivity of 1.4×10^{-5} S cm^{-1}. Yubuchi et al. reported a liquid-phase technique for the preparation of argyrodite-type Li_6PS_5Br with a lithium-ion conductivity of 1.9×10^{-4} and 3.1×10^{-3} S cm^{-1} via a homogeneous ethanol solution and a THF, respectively.[66–67] THF was used as the solvent for the synthesis of Li_6PS_5X because it shorter reaction time compared with 1,2-dimethoxyethane (DME) or ACN.[44] Recent reports using liquid-phase method can synthesize the Li_6PS_5Cl and mixed anion Li_6PS_5 (Cl, Br) argyrodites with the ionic conductivity up to 2.4 and 3.9×10^{-3} S cm^{-1}, respectively.[44]

Low ionic conductivity is the main drawback for the liquid-phase method, which may cause by the contamination from the organic solvent. However, the liquid-phase method can facilitate solid electrolytes coat on the active material to form a favorable solid-solid interface thus improving cell performance. Therefore, liquid-phase synthesis methods have been adopted to reduce the electrode/electrolyte interfacial resistance, which will be discussed in Section 3.2.1.

As shown in **Figure 5**, the parameter selection in all synthesis methods is also important in determining the property of electrolyte. For example, the reaction atmosphere and cooling speed for solid state methods, ratio of balls and power and milling time for high energy milling methods and additive types and solvents for liquid-phase methods need to be optimized to obtain a high ionic conductivity. The ionic conductivities of typical sulfide electrolytes prepared by different methods are summarized in **Table 1**. In summary, ball-milling is an essential process for synthesizing sulfide solid glass–ceramic electrolytes. During the high-energy milling, the mixing and pulverization processes occur at the same time. More importantly, amorphous electrolytes can be realized at room temperature through ball-milling. However, for the crystalline ones, such as $Li_{10}GeP_2S_{12}$ and Li_6PS_5X, the ionic conductivity of these electrolytes prepared by high energy milling are lower than those synthesized by high-temperature solid reaction or liquid process.

2.3. Electronic Conductivity of the Sulfide Electrolytes

ASSLBs are widely considered to adopt lithium metal as anode because the solid electrolytes are believed can suppress Li dendrite growth. However, recent reports showed that the Li dendritic issues in the sulfide electrolytes are more complicated.[72–75] Lukas et al. found that the Li was plated at the defects of the $70Li_2S$–$30P_2S_5$, which is inconsistent with the Monroe–Newman model for explaining "dendrites." Their results suggested that minimizing the interfacial defects such as void or grain boundary is highly required for avoiding lithium metal penetration.[74] However, recently, Han et al. found that the Li

Table 1. The ionic conductivities of typical sulfide electrolytes prepared by different methods.

Electrolyte	Ionic conductivity [S cm^{-1}]	Preparation method	Ref.
Thio-LSICON			
Li_3PS_4	6.4×10^{-6}	Shaking in Ar	[51]
β-Li_3PS_4	1.6×10^{-4}	Liquid phase (THF)	[23]
	3×10^{-2} S cm^{-1} (500 K)	Solid-state methods	[25]
γ-Li_3PS_4	3×10^{-7}	Solid-state methods	[25]
Amorphous Li_3PS_4	2×10^{-4}	High-energy ball milling	[19]
Li_3PS_4	$\approx 10^{-3}$	Mechanical milling	[69]
	2.3×10^{-6}	Liquid phase (DMF)	[64]
$Li_7P_3S_{11}$	3.2×10^{-3}	Mechanical milling	[21]
	7.3×10^{-3}	Solid-state method (hot pressed)	[53]
	5.2×10^{-3}	Solid-state method (hot pressed)	[56]
	1.7×10^{-2}	Solid-state method (hot pressed)	[11]
	2.7×10^{-3}	Liquid phase (DME)	[59]
	1×10^{-3}	Liquid phase (acetonitrile)	[60]
	9.7×10^{-3}	Liquid phase (THF/ACN/THF&ACN)	[61]
	8.7×10^{-4}	Liquid phase (ACN)	[63]
LGPS-type			
$Li_{10}GeP_2S_{12}$	1.2×10^{-2}	Solid-state method	[5]
	6.3×10^{-3}	Solid-state method	[69]
$Li_{10}SnP_2S_{12}$	4×10^{-3}	Solid-state method	[31–32]
$Li_{9.54}Si_{1.74}P_{1.44}S_{11.7}Cl_{0.3}$	2.5×10^{-2}	Solid-state method	[6]
Li_7GePS_8	7×10^{-3}	Solid-state method	[29]
Li_6PS_5X (X = Cl, Br, I)			
Li_6PS_5Cl	6.2×10^{-4}	High-energy ball milling	[43]
	1.18×10^{-3}	Solid-state method	[48]
	4.96×10^{-3}	Solid-state method	[58]
	1.4×10^{-5}	Liquid phase (ethanol)	[65]
	6×10^{-5}	Liquid phase (mixture of solvents)	[70]
	2.4×10^{-3}	Liquid phase (mixture THF and ethanol)	[44]
Li_6PS_5Br	6.2×10^{-4}	High-energy ball milling	[43]
	1.9×10^{-4}	Liquid phase (ethanol)	[66]
	1.9×10^{-3}	Liquid phase	[44]
	3.4×10^{-5}	Liquid phase (thyl propionate-ethanol solution)	[71]
Li_6PS_5I	1.9×10^{-4}	High-energy ball milling	[43]
$Li_{5.5}PS_{4.5}Cl_{1.5}$	9×10^{-3}–1.2×10^{-2}	Solid-state method	[46]
$Li_{6+x}P_{1-x}Ge_xS_5I$	5.4×10^{-3}–1.8×10^{-2}	Solid-state method	[47]
$Li_6PS_5Cl_xBr_{1-x}$	$\approx 3 \times 10^{-3}$	Liquid phase	[44]
$Li_{5.75}PS_{4.75}Cl_{1.25}$	3.0×10^{-3}	Liquid phase	[44]
$Li_{5.5}PS_{4.5}Cl_{1.5}$	3.9×10^{-3}	Liquid phase	[44]

dendrites still grow in a very dense $Li_7La_3Zr_2O_{12}$. In addition, the dendrite formation in the grain boundary is not improved by increasing its ionic conductivity in grain boundary. No clear theory can reconcile all these dendrite formations in solid electrolytes. They quantified the net amount of Li transported from Li and compared with the cumulative electric charge, and suggested that the other most important factors for the Li dendrite formation in sulfide electrolyte is the high electronic conductivity. Therefore, for inhibiting the dendritic formation of the ASSLBs, lowering the electronic conductivity is more important than increasing the ionic conductivity of solid electrolytes.[76] **Table 2** list the electronic conductivity of the sulfide electrolytes. Dopants, grain boundaries or electrochemical reductions should be reduced to guarantee the lithium metal anode can be really applied in ASSLBS based on sulfide electrolytes.

2.4. Electrochemical Stability Window of Sulfide Electrolytes

The electrochemical stability window of solid electrolytes is an important factor for the performance of lithium battery. The liquid organic electrolytes always present instability at high voltage >4.5V versus Li/Li$^+$ and normally form a solid electrolyte interphase (SEI) at the surface of the anodes and cathode electrolyte interphase (CEI) on cathodes, which helps to extend the electrochemical stability window. However, the formation of SEI

Table 2. The ionic and electronic conductivities of typical sulfide electrolytes prepared by different methods.

Electrolyte	Ionic conductivity [S cm^{-1}]	Electronic conductivity [S cm^{-1}]	Preparation method	Ref.
Amorphous $60Li_2S{\cdot}40SiS_2$	1.4×10^{-4}	$<10^{-8}$	High-energy ball milling	[77]
$Li_{3.25}Ge_{0.25}P_{0.75}S_4$	2.17×10^{-3}	2.6×10^{-9}	Solid-state reaction	[27]
Li_3PS_4	$\approx10^{-3}$	2.2×10^{-9}	Mechanical milling	[76]
Amorphous Li_3PS_4	2×10^{-4}	6.3×10^{-9}	High-energy ball milling	[19]
Li_3PS_4	$\approx10^{-3}$	$\approx10^{-8}$	Mechanical milling	[69]
$Li_{10}GeP_2S_{12}$	1.2×10^{-2}	5.7×10^{-9}	Solid-state reaction	[5]
$Li_{10}GeP_2S_{12}$	6.3×10^{-3}	$\approx10^{-8}$	Solid-state reaction	[69]
Li_6PS_5Cl	6.2×10^{-4}	4×10^{-9}	High-energy milling	[43]
	2.4×10^{-3}	5.1×10^{-9}	Liquid phase	[44]
Li_6PS_5Br	4.6×10^{-4}	2.6×10^{-8}	High-energy milling	[43]
	1.9×10^{-3}	4.4×10^{-9}	Liquid phase	[44]
Li_6PS_5I	1.9×10^{-4}	2.4×10^{-8}	High-energy milling	[43]
$Li_6PS_5Cl_{0.75}Br_{0.25}$	3.2×10^{-3}	3.7×10^{-9}	Liquid phase	[44]
$Li_6PS_5Cl_{0.5}Br_{0.5}$	3.9×10^{-3}	1.4×10^{-8}	Liquid phase	[44]
$Li_6PS_5Cl_{0.25}Br_{0.75}$	3.4×10^{-3}	1.1×10^{-8}	Liquid phase	[44]
$Li_{5.75}PS_{4.75}Cl_{1.25}$	3.0×10^{-3}	2.6×10^{-8}	Liquid phase	[44]
$Li_{5.5}PS_{4.5}Cl_{1.5}$	3.9×10^{-3}	1.4×10^{-8}	Liquid phase	[44]

will also consume the electrolyte and introduce a large interfacial resistance. Unlike the passivation SEI layers in the liquid electrolytes, which are electron-insulating and ion-conducting, the SEIs in solid state devices may be electronically conductive, which will continuously grow during cycling and destroy the capacity of the cells.[39] There are also some evidence that the decomposition product of sulfide electrolytes like Li_6PS_5Cl,[78] Li_3PS_4,[79–81] and $Li_{10}GeP_2S_{12}$[82] are electrochemically active, which prove the importance for identify the real reaction of solid electrolyte with electrodes during cycling. The poor interfacial contact, space charge layer, and chemical interaction between electrode and electrolyte are considered as the main reason for the increased resistance.[83–84]

The electrochemical stability window of solid electrolytes is normally measured in a Li/electrolyte/inert metal (stainless or Pt) blocking electrode using cycling voltammetry as shown in **Figure 6**. Sylvain et al. evaluated the electrochemical stability of a series of Li_6PS_5X (X = Cl, Br, I) argyrodites with a stainless steel/BM-Li_6PS_5X/Li cell. It seems that the electrolytes can maintain stable in the voltage of 0.5–7V versus Li/Li$^+$.[43] The sulfide electrolytes like $Li_7P_{2.9}Mn_{0.1}S_{10.7}I_{0.3}$ and $Li_{9.54}Si_{1.74}P_{1.44}S_{11.7}I_{0.3}$ exhibited a wide voltage stability up to 5 V and 9 V (vs Li/Li$^+$) tested by the same methods.[22,38]

Han et al. demonstrated that the electrochemical stability window measured using semiblocking electrode is wider than true stability window because the poor contact between electrolyte and semiblocking electrode reduce reaction kinetics lowering the sensitivity.[85] The first-principles was used to predict the electrochemical stability windows and fount the much smaller stability window than the experimentally reported values as shown in **Figure 7**.[84] The discrepancy caused between the calculated and experimentally measured values was corrected by increasing the contact area of solid electrolyte and current collector using a Li/electrolyte/electrolyte-carbon cell, through which the intrinsic stability window of the solid electrolytes can be approached.[85] Therefore, extending the electrochemical window of the solid electrolytes should be addressed to avoid the high interfacial resistances caused by the decomposition of solid electrolytes.

2.5. Chemical Stability with Humid air and Organic Solvent

Besides the electrochemical stability, the chemical stability of the solid electrolyte is another important factor to influence the

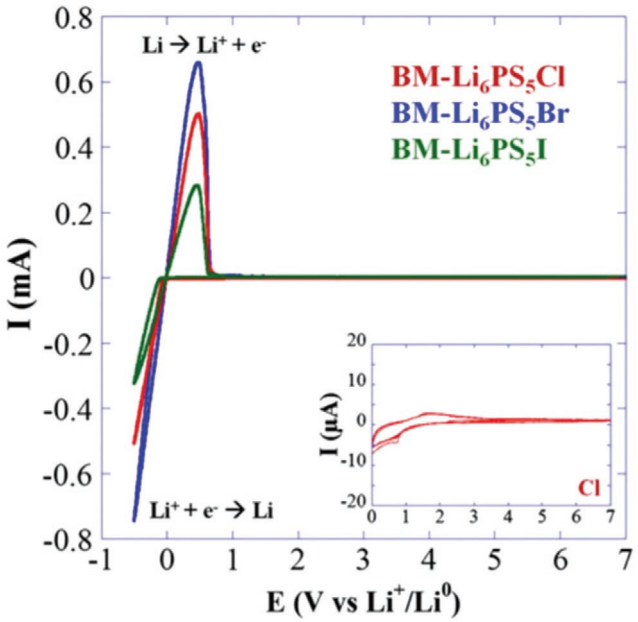

Figure 6. Cyclic voltammetry of a stainless steel/Li_6PS_5X/Li cell. Reproduced with permission.[43] Copyright 2012, Elsevier.

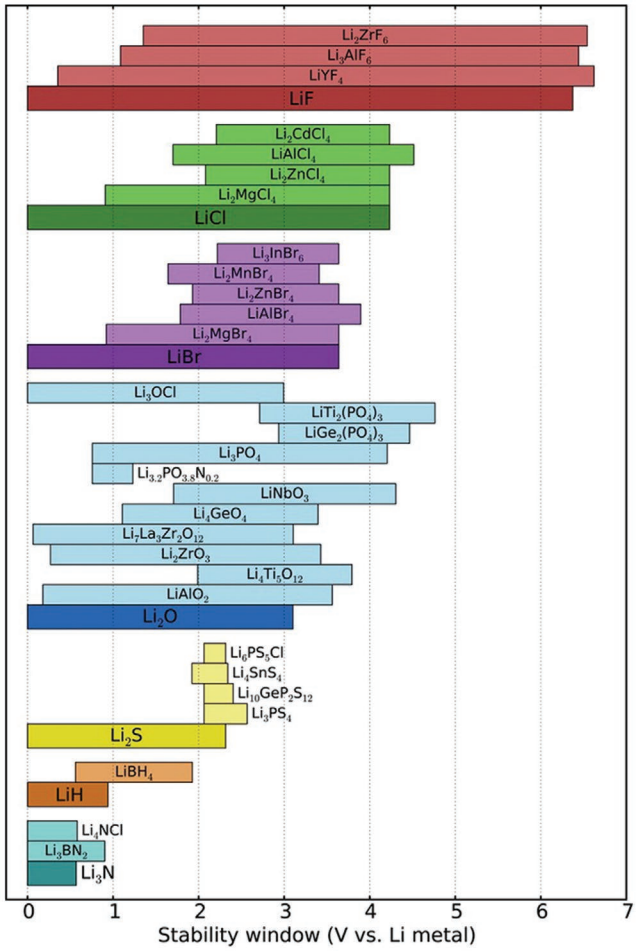

Figure 7. Electrochemical stability ranges of various electrolyte materials. Reproduced with permission.[84] Copyright 2015, American Chemical Society.

electrochemical performance of ASSLBs. The high sensibility of the sulfide electrolytes to moisture make the preparation process operated in the inert gas. H_2S gas evolution is an obvious sign for testing the hydrolyses of the sulfide electrolytes. Muramatsu et al.[24] studied the chemical stability of the Li_2S–P_2S_5 in an ambient atmosphere. Among the well-known thio-LISICON type electrolytes and the LGPS electrolytes, Li_3PS_4 was found more stable than the others when exposed in air primarily due to the higher stability of PS_4^{3-} compared with other phosphate ions. To reduce the sensitivity of the sulfur electrolytes for moisture, a series of additives including M_xO_y (M_xO_y: Fe_2O_3, ZnO, and Bi_2O_3) and halide (LiCl, LiBr, LiI) have been added.[86] The suppression mechanism of oxide as the adsorbent to suppress the H_2S is proceeded via the following reaction

$$M_xO_y + H_2S \rightarrow M_xS_y + H_2O \quad (2)$$

Recently, the stability of LiI, LiCl, and P_2O_5 doped Li_3PS_4 in ambient atmosphere was also explored in our group. In our experiments, as shown in **Figure 8**a, the Li_3PS_4 and $99Li_3PS_4$–$1P_2O_5$ showed the best stability. A generation of minimum H_2S gas in 40 min can be tested.[87] In addition, Sn- and As-based sulfide electrolytes are found of high air-stability. Because the As and Sn are intended to form stable compound which can resist hydrolysis and oxidation based on the acid and base theory.[88]

In addition to chemical stability with the moisture in the air, chemical stability of solid electrolyte with solvents is also important when the solid electrolyte is synthesized using liquid method due to the merits of low cost and convenience. In addition, the liquid methods are thought to be beneficial for constructing electrolyte/electrode interface. Although significant progresses have been made in the stability of sulfide electrode in organic solvents,[89–90] establishing a better understanding of the mechanism on sulfide electrolytes against solvents is still critical. The stability of sulfide electrolytes including Li_3PS_4 (LPS), $90Li_3PS_4$–$10LiI$ (LPS–I), $90Li_3PS_4$–10LiCl (LPS–Cl), and $99Li_3PS_4$–$1P_2O_5$ (LiPS–O) in ACN, cyclohexanone (CYC), and chlorobenzene (ClB) was tested. ACN, ClB and CYC are the commonly used solvents for synthesis of the sulfide electrolyte. In addition, they are volatile solvents that facilitate evaporation of the solvent during battery manufacturing. As shown in Figure 8b–d, as the time increases, the ionic conductivity of all these electrolytes decrease. Among all these electrolytes, the Li_3PS_4 are more stable compared with other electrolytes. The sulfide electrolytes are more stable in ClB solvent rather than in the other solvents due to its highly stable benzene ring. In addition, toluene and *n*-heptane were found suitable as solvent to disperse solid electrolyte due to their high stability with sulfide electrolyte.[91–92] Nam et al.[92] prepared a bendable and thin sulfide electrolyte films through liquid method, using toluene as solvent. No obvious side reactions were found in the preparation process, which may imply toluene can be used as solvent in preparing solid electrolyte films due to its high stability with sulfide electrolyte.

3. Sulfur-Based Cathodes

3.1. Fundamentals for Cathode/Electrolyte Interface

One of the most important factors for the electrochemical activity of ASSLBs is the interfacial stability, which can be further divided into electrochemical, chemical and physical contact stability. First, the electrochemical stability of solid electrolyte can be estimated by the stability window which can be determined by the energy separation E_g. E_g is calculated between the lowest unoccupied molecular orbital (LUMO) or conducting band (CB) and the highest occupied molecular orbital (HOMO) or valence band (VB) of the electrolyte material. When the chemical potential (μ_a for anode and μ_c for cathode) of the electrode materials is within the LUMO–HOMO range, the interface is thermodynamically stable (**Figure 9**a,b)). Otherwise, the interface is not stable if μ_a > LUMO (or CB) or μ_a < HOMO (or VB), unless an SEI forms at the interface (Figure 9c).[93] Second, the chemical reaction between solid electrolyte and cathode also enhances the interface resistance. Third, unlike the liquid-electrolyte system, wherein the electrode is fully infiltrated by a liquid electrolyte, in ASSLBs, the physical stability is important because the charge-transfer is limited to the triple-phase points (the phase between active material, electronic additive,

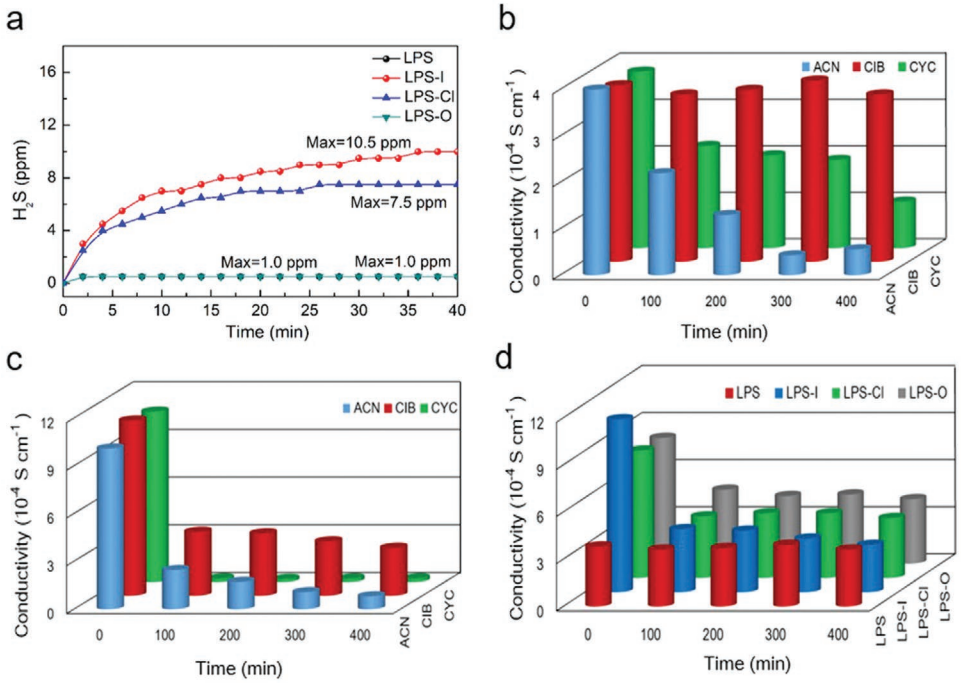

Figure 8. The chemical stability of sulfide electrolyte with humid air and organic solvent. a) Time dependence of H_2S amounts released from the Li_3PS_4 (LPS), $90Li_3PS_4$–$10LiI$ (LPS–I), $90Li_3PS_4$–$10LiCl$ (LPS–Cl), and $99Li_3PS_4$–$1P_2O_5$ (LPS–O) composites in humid air. b,c) Variations of the conductivities for LPS (b) and LPS-I (c) in different solvents. d) Variations of conductivities for different sulfide electrolytes in ClB solvents. a–d) Reproduced with permission.[87] Copyright 2018, Elsevier.

and ionic conductor).[94] During repeating volume expansions and contraction of active material, the triple-phase points will decrease in the cathode and cracks will be formed at cathode/electrolyte interface, leading to increased interfacial resistance. Different from oxide cathode, sulfide cathodes show better compatibility and similar chemical potential with sulfide electrolyte. Therefore, for sulfide cathode, the main challenge restricting the stability of cathode/electrolyte interface is the stress/strain generated due to the volume change of the electrodes.

Due to the point contacts between the solid electrolytes and solid electrodes at the interface of ASSLBs, the limited active sites are always accompanied by the large interface resistance,

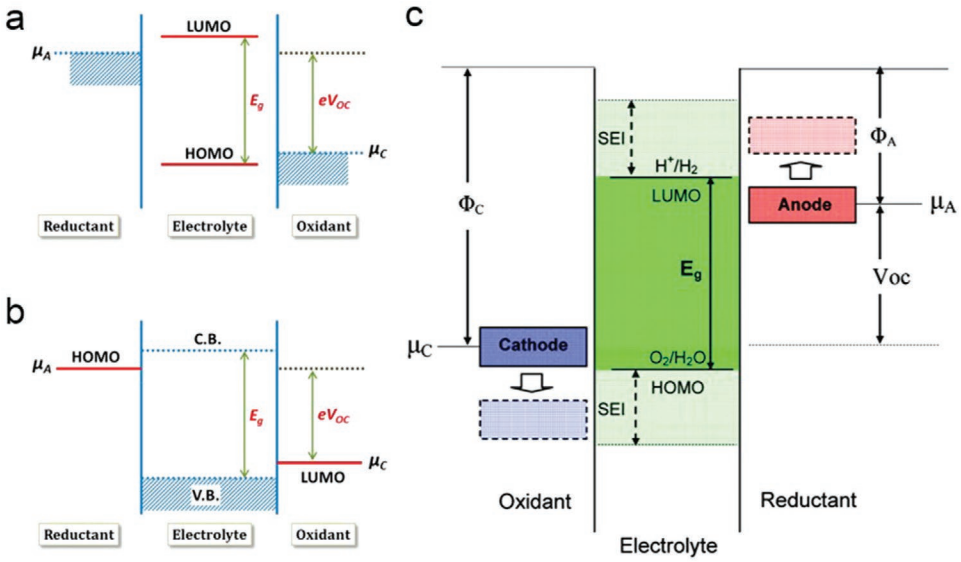

Figure 9. Open-circuit energy diagrams of different battery systems. a) Overall illustration of a battery with a liquid electrolyte. b) Stable energy window for liquid electrolyte. a,b) Reproduced with permission.[95] Copyright 2013, American Chemical Society. c) Stable energy window for solid electrolyte. Reproduced with permission.[96] Copyright 2010, American Chemical Society.

which will further lead to the degradation of the battery performance. A stable interface, including close contact between the active material, conductive agent, and the solid electrolyte, is necessary to facilitate smooth flow of ions and electrons throughout the electrode. Constructing buffer layer is effective to reduce the interfacial impedance. Many strategies are proposed to form a stable interfacial layer between the electrolytes and the electrodes. However, the selection criteria, the construction methods, the structure, and the effect of the buffer layers are still unclear. More investigations are needed for this area.

3.2. Strategies to Form Intimate Cathode/Electrolyte Interface

In bulk-type ASSLBs, an electrode is a mixture of three constituents of active materials, solid electrolytes, and conductive additives. Electrochemical reactions proceed at the solid–solid interface and are affected by the states of the interface in the electrode. More importantly, the inhomogeneous solid–solid contact between electrode and electrode with poor wetting can generate large interface impedance. In order to enhance the interfacial ion transfer and suppress the interfacial reactions, a great number of strategies have been proposed for tackling the issues of interface between cathodes and electrolyte.

3.2.1. In Situ Liquid-Phase Approach

The liquid-phase method is simpler than the gas-phase method for coating solid electrolytes on solid electrodes. The intact interfaces between solids electrodes and liquid electrolyte precursor solution are easily formed. After removing the organic solvents, a layer of homogeneous solid electrolytes can be formed on the surface of the cathodes.

Yao et al.[62] reported an interfacial architecture that sulfide electrolytes were coated on Co_9S_8 nanosheets through an in situ liquid process. **Figure 10** schematically outlined the experimental procedure. First, Co_9S_8 nanosheets were synthesized through an aqueous precipitation reaction. After that, Li_2S and P_2S_5 were added in cobalt sulfide solution, resulting in the Co_9S_8–$Li_7P_3S_{11}$ nanocomposites precursor. The morphology of the composite electrode showed that the anchored sulfide electrolyte particles are about 10 nm, which is obviously smaller compared with that produced by the solid state methods, leading to an increased contact area between the electrolyte and Co_9S_8 nanosheets. A good lithium-ion conduction path thus can be formed which greatly reduces the interfacial resistance. ASSLBs employing cobalt sulfide–$Li_7P_3S_{11}$ nanocomposites present exceptionally long cycle stability. After 1000 cycles, the reversible capacity is 421 mAh g^{-1} at 1.27 mA cm^{-2}. In addition, the obtained battery also presents very high energy and power densities, which are 360 and 3823 W kg^{-1} at 0.13 and 12.73 mA cm^{-2}, respectively. This result provides a new interfacial design strategy for ASSLBs with high performances, which is also can be considered as a general method for synthesis of other composites cathode for ASSLBs. After that, they reported a Fe_3S_4@$Li_7P_3S_{11}$ nanocomposite using the same method.[97] ASSLBs employing the Fe_3S_4@$Li_7P_3S_{11}$ nanocomposite deliver a higher discharge capacity than that of the pristine Fe_3S_4 nanosheets. The cycling ability was also greatly enhanced, which can maintain a stable value of 1001 mAh g^{-1} within 200 cycles. The improved capacity and cycle stability can be attributed to the intimate contact between cathode and solid electrolytes. Similarly, Tu et al.[98] reported a uniform coating of $Li_7P_3S_{11}$ on MoS_2 by a liquid-phase approach. The interfacial resistance of the interface was greatly improved by the compact contacting between MoS_2 nanosheets and $Li_7P_3S_{11}$ particles. ASSLBs employing MoS_2/$Li_7P_3S_{11}$ composite as the cathode exhibited enhanced electrochemical activity. An initial capacity of 868.4 mAh g^{-1} at 0.1 C and a high reversible capacity of 547.1 mAh g^{-1} within 60 cycles can be obtained.

3.2.2. Solution Bottom-Up Method

Several barriers, which include but are not limited to the low sulfur utilization, poor cycling stability, and low rate capability, exist in commercializing ASSLBs. The volume change and low electronic/ionic conductivities of S and Li_2S are proposed as the main reasons

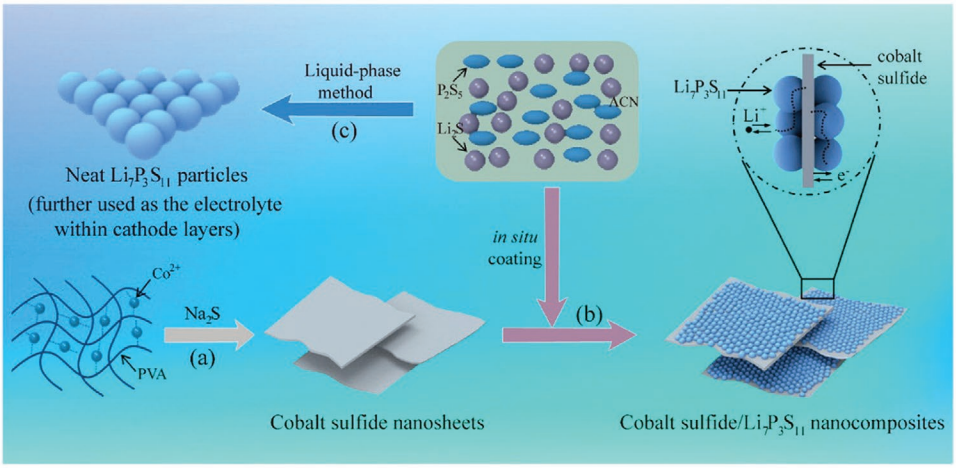

Figure 10. Schematic for preparation of cobalt sulfide–$Li_7P_3S_{11}$ nanocomposites, and $Li_7P_3S_{11}$ electrolyte. Reproduced with permission.[62] Copyright 2016, American Chemical Society.

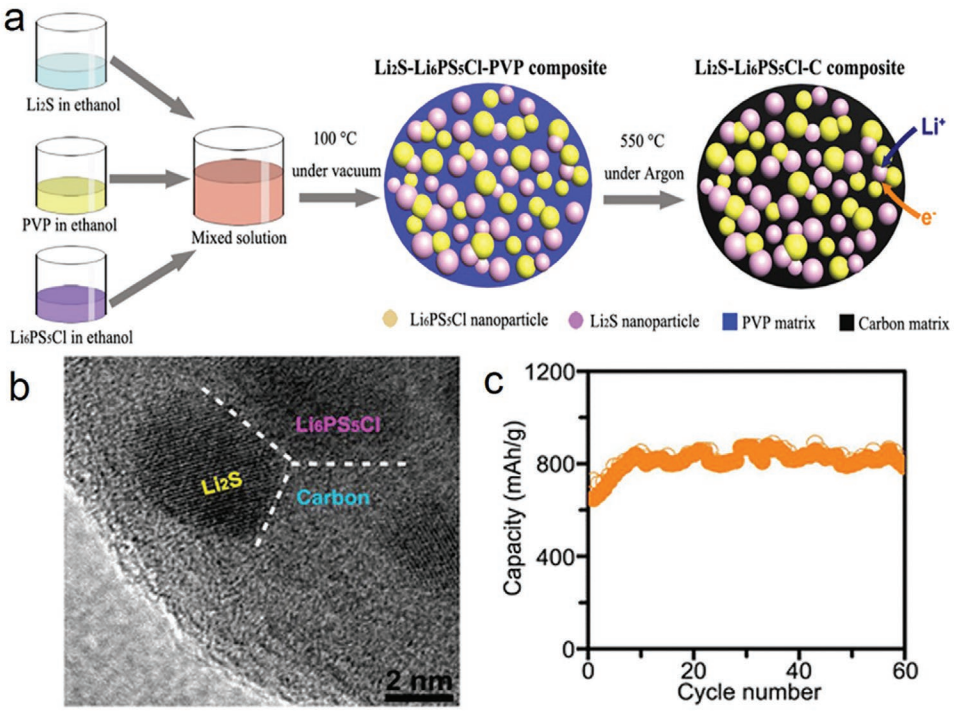

Figure 11. a) Schematic for fabrication the Li_2S nanocomposite. b) TEM image of the as-obtained Li_2S–Li_6PS_5Cl–C nanocomposite. c) Cycling performances of the Li_2S–Li_6PS_5Cl–C at 50 mA g^{-1}. a–c) Reproduced with permission.[99] Copyright 2016, American Chemical Society.

for the inferior electrochemical activity. One of the most attractive strategies to mitigate these challenges is synthesis of a sulfur nanocomposite electrode with nanoscale size and homogeneous distribution of active material, solid electrolyte, and conductive agent. Han et al.[99] proposed a bottom-up method by dissolving Li_2S, polyvinylpyrrolidone, and Li_6PS_5Cl in ethanol, followed by a coprecipitation and carbonization process, the schematic is shown in **Figure 11**a. When the Li_2S and Li_6PS_5Cl with nanoscale in situ grown in the soft carbon matrix (Figure 11b), the nanocomposite could provide buffer space, which not only alleviate the strain/stress in charge/discharge process, but also promotes the fast Li-ion transfer. In addition, the carbon is an excellent electronic conductor, combined with the homogeneous distribution of the active material and electrolytes, exhibiting the large triple-phase contact, which is believed to utilize the active material at the high level. Consequently, the Li_2S–Li_6PS_5Cl–C nanocomposite ensures a better structure which not only allows sufficiently fast Li-ion and electron kinetics but also accommodates the volume change during the delithiation/lithiation process. A large discharge capacity of 830 mAh g^{-1} within 60 cycles and excellent rate performance thus can be obtained. The simple approach proposes a new strategy for synthesis homogeneous electron/ion conducting nanocomposite cathode for high-performance ASSLBs.

3.2.3. Pulsed Laser Deposition (PLD) Technique

PLD is a kind of film deposited technique using pulsed laser to strike a target material. As the laser energy is very strong, it will vaporize the target material to form a plasma-like mass, and precipitate on the substrate to form a film.[100] Many materials that are normally difficult to deposit by other methods have been successfully handled by PLD.[101] A series of studies were conducted by Tatsumisago's group to reduce the interface impedance for ASSLB using the PLD technique. For example, ternary composite cathode including NiS, sulfide electrolytes, and vapor grown carbon fiber (VGCF) was successfully synthesized through this PLD method. In this method, a pelletized $80Li_2S$–$20P_2S_5$ electrolyte was used as deposition target. During the deposition process, the electrolyte was fluidized to form a uniform SE layer on the NiS–VGCF composite. The schematic illustration is shown in **Figure 12**. Therefore, intimate interfaces among NiS, VGCF, and SEs were obtained, giving favorable electronic (VGCF) and lithium ion conduction ($80Li_2S$–$20P_2S_5$ electrolyte) pathway to NiS nanoparticles, leading higher electrochemical activity than that of the uncoated NiS–VGCF composite. The ASSLB using the SE-coated NiS–VGCF composite cathodes exhibited a high discharge capacity of 300 mAh g^{-1} (3.8 mA cm^{-2}) and better cycle performance than that uncoated composite, which should attribute to the favorable NiS–VGCF–SE interfaces.[102]

More importantly, this method can be extended to coat proper electrolyte on cathodes such as Li_2S–P_2S_5@$LiCoO_2$,[103–104] Li_3PO_4@$LiNi_{0.5}Mn_{1.5}O_4$. After coating Li_3PO_4 buffer layer on the LNMO surface by PLD, the interface impedance between sulfide electrolyte and LNMO/Li_2S–P_2S_5 cathode was greatly reduced, resulting in enhanced rate ability.[105]

3.2.4. Ball Milling

Mechanical ball-milling is another method for mixing electrolytes and cathodes. The mechanical ball-milling is able to run

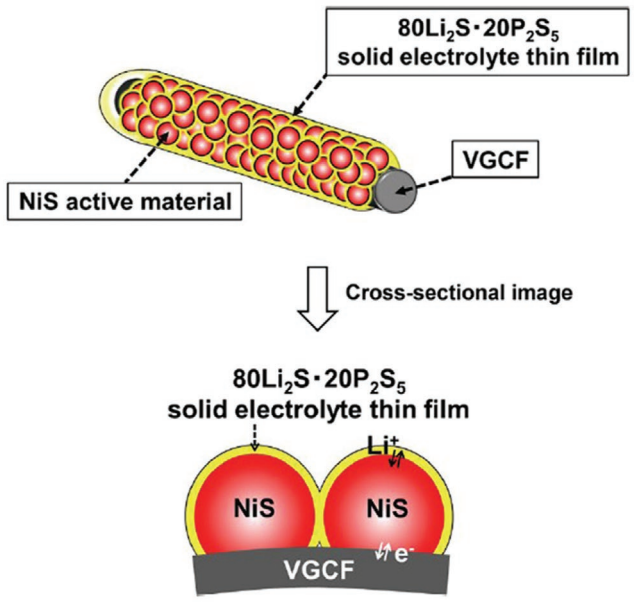

Figure 12. Schematic of the SE-coated NiS-VGCF composite (SE denotes the $80Li_2S{\cdot}20P_2S_5$ (mol%) solid electrolyte). Reproduced with permission.[102] Copyright 2013, American Chemical Society.

continuously thus permitting scaled production in industry. The amorphous materials can also be obtained by ball-milling which is difficult to realize by the conventionally solid-state methods.

Jung et al. investigated electrochemical performance of TiS_2 and Li_2S–P_2S_5 nanocomposite as cathode for ASSLBs.[106] The composites prepared by the ball-milling present higher charge capacity of 837 mAh g^{-1} and better capacity retention of 95% within 60 cycles compared to which prepared by manually mixed method. As shown in **Figure 13**a, the TiS_2 and sulfide electrolyte in nanoscale prepared by the ball-milling can make intimate contacts between them. Furthermore, the ball-milling is facilitated to the formation of amorphous phases of Li–Ti–P–S which provide the sufficient ionic and electronic transfer pathways. More importantly, the origin of the extra Li storage is verified to associate with the formation of Li–Ti–P–S phase. The high-resolution TEM image of the as-obtained TiS_2-electrolyte composite are shown in Figure 13b. This strategy can be extended to other systems for ASSLBs. Therefore, the controlled ball-milling is considered as an efficient method for significantly improving the energy density of ASSLBs.

Tatsumisago et al. prepared S–acetylene–$80Li_2S$–$20P_2S_5$ (S–AB–SE) composite cathode via ball-milling.[107] S was first ball-milled with AB to form S–AB composite. Then, S–AB composite was further milled with SEs to obtain S–AB–SE composite cathode. The amorphous nature of sulfur in the obtained S–AB–SE composite can increase the capacity of lithium–sulfur battery. Besides, the decreased particle size of the component materials in S–AB–SE composite can promote the intimate contacts between S, AB, and SEs. Therefore, the ASSLB employing S–AB–SEs composite exhibited excellent cycling performance and a wide operation temperature (–20–80 °C). It was concluded that the intimate contact between the electrode components by the ball-milling treatment was effective for increasing the capacity of an ASSLB. Tu et al. also synthesized a sulfur-based cathode by mixing sulfur and carbon black to form S–C composite, then further milling S–C composite with $Li_7P_{2.9}Mn_{0.1}S1_{0.7}I_{0.3}$ and $Li_7P_{2.9}S_{10.85}Mo_{0.01}$ electrolyte to obtain S–C–$Li_7P_{2.9}Mn_{0.1}S1_{0.7}I_{0.3}$ and S–C–$Li_7P_{2.9}S_{10.85}Mo_{0.01}$, composite, respectively.[22,108]

3.2.5. Others

Nanocrystallization of the electrode is widely applied to show enhanced electrochemical performance due to the reduced diffusion paths. Furthermore, for the ASSLB the nanocrystallizaiton can improve the contact at the electrode/electrolyte interface. According to the diffusion formula: $t = L^2/D$ (L: diffusion length, D: diffusion constant), which means decrease particle size could reduce reaction time greatly.[109] Moreover, the higher surface energy enable electrode reactions to occur that cannot take place for micrometer-sized particles.[110] In addition, high surface area means high contact area and thus a large amount of active sites for the electrochemical reaction. Therefore, nanostructured materials have been extensively explored in efforts to enhance the kinetic properties

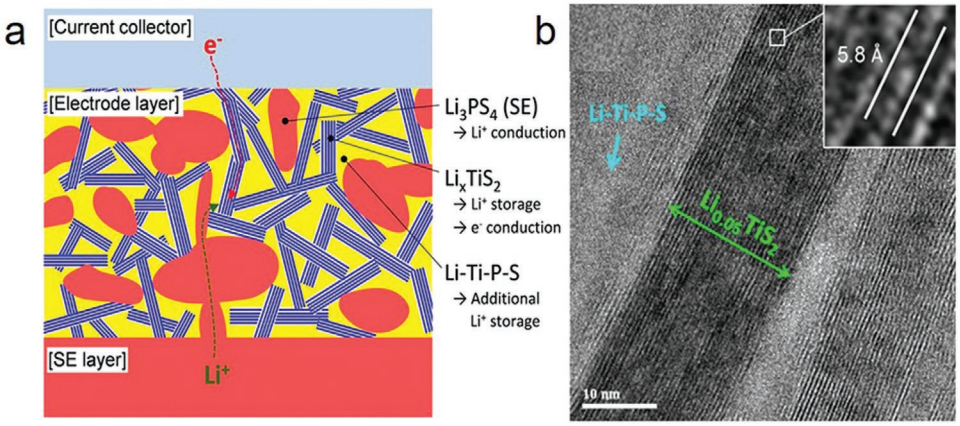

Figure 13. a) Schematic illustration of the microstructure composite cathode in ASSLB. b) The TEM image of the as-obtained TiS_2–electrolyte composite prepared by ball-milling. a,b) Reproduced with permission.[106] Copyright 2014, Springer Nature.

for solid-state lithium batteries. Modifying the electrode with carbon materials is another strategy to improve electrochemical performances. Among the diverse carbon materials, CNT and graphene have been widely used to better the electrochemical performance of the cathode materials used for ASSLBs. Moreover, their unique low dimensional structures are favorable to form conductive networks. Furthermore, the carbon matrixes accommodate the large change in volume and act as a conducting media simultaneously. Therefore, reduction of particle size and composite with carbon materials are effective to improve the cathode/electrolyte interface contact, and maintain structure stability, thus delivering enhanced electrochemical performance.

Long et al.[111] prepared an ASSLB employing NiS nanorods as cathode. The electrochemical performance showed that the nanosized NiS exhibited enhanced capacity and cycle stability. The significantly reduced particles are beneficial for the interface contact, thus improving the utilization of active materials and charge transfer kinetics. Zhang et al.[112] synthesized a NiS–CNT composite by anchoring NiS nanoparticles on CNT surface. The nanosized NiS as well as the presence of high conductive CNT not only enhanced the ionic/electronic conductivity but also alleviated the stress/stain during charge/discharge process. The ASSLBs employing the NiS–CNT as cathodes delivered an excellent cycling performance of 170 mAh g^{-1} with 150 cycles.

3.3. Sulfur-Based Electrode Materials

3.3.1. Sulfur

Elemental sulfur has high theoretical capacity (1675 mAh g^{-1}). More importantly, sulfur does not suffer from polysulfide dissolution in SEs.[113–114] Tataumisago's group first reported the use of sulfide-based solid electrolyte for solid state Li–S batteries. The S@CuS composite cathode was prepared by mechanical milling. ASSLB using the sulfur-based cathode materials and the Li_2S–P_2S_5 electrolytes delivered a large reversible capacity of 650 mAh g^{-1} within 20 cycles, where S and CuS both worked as an active materials.[115] Particle size the sulfur plays an important role for high charge-discharge capacities. Kanno's group reported a nanocomposite electrode of sulfur and acetylene black (AB) fabricated through gas-phase mixing followed by mechanical balling. Particle size of sulfur after gas/solid mixing was 1–10 nm, leading to an intimate contact interface between sulfur and AB, which improve the sulfur utilization. The extremely high capacity obtained for the composite electrode was due to the close contact between sulfur and AB which acts as conducting matrix. In addition, this gas/solid mixing method leads to the low resistivity of the composites indicated by the impedance spectroscopy.[116] Afterward, they prepared a similar ASSLB using mesoporous carbon (CMK-3) as the conducting matrix. The high electrical conduction path way and sulfur utilization can be realized simultaneously by the special mesoporous framework of CMK-3. Electrochemical test showed that the S/CMK-3 nanocomposite cathode delivered a large initial capacity of 1600 mAh g^{-1} capacity and excellent rate performance attribute to the intimate contact between nanosized sulfur and conducting carbon matrix.[117] Similarly, Sakuda et al.[118] reported a composite cathode using interconnected mesoporous carbon as an effective sulfur host. The highly interconnected carbon helps the formation of an excellent electronic pathway, thus improving electrode kinetics. Consequently, the ASSLSB employing this composite cathode delivered an excellent capacity of over 1100 mAh g^{-1} for 400 cycles at a high current density of 1.3 mA cm^{-2}. Nagata et al.[119] investigated the relationship between the conductive sulfur host and battery performance. Their results showed that the surface area of the conductive host plays a more important role than the intrinsic electronic conductivity of the host in the electrochemical performance of ASSLSBs. ASSLSBs employing activated carbon composite cathode with a high surface area exhibited a high reversible capacity of over 1600 mAh g^{-1} for 100 cycles at high rate of 1C, and a high power density over 11 000 W kg^{-1} at 50% state of charge. All these finding showed that the mesoporous carbon especially that with high surface area are promising as the sulfur host for practical ASSLSBs.

More recently, Yao et al.[120] reported an all-solid-state lithium–sulfur battery (ASSLSB) employing the bilayered $Li_{10}GeP_2S_{12}$/75%Li_2S–24%P_2S_5–1%P_2O_5 as electrolyte and the rGO modified S as cathode, as shown in **Figure 14**a. Herein, the interface resistance between the cathodes and the electrolyte is significantly reduced by coating a nanolayer of S on the rGO, which was demonstrated by the atomic force microscopy (AFM) pattern (Figure 14b). The obtained ASSLBs exhibit an initial discharge capacity of 1629 mAh g^{-1} and high rate capability from 0.05 to 5 C (Figure 14c,d). The excellent capacity retention of high rate capabilities is attributed to the avoidance of polysulfide shuttle and alleviation of the volume variation during the charge/discharge process. Afterward, CNTs@S nanocomposites were reported by depositing sulfur on the surface of CNTs though a thiamine method.[121] The ASSLSB with this mixing cathode exhibited excellent rate capability and ultralong cycle stability at 60 °C. Moreover, the CNTs@S constantly delivered a capacity of 660.3 mAh g^{-1} within 400 cycles at a rate of 1.0 C. In the cathode structure, the CNTs provided high electronic conductivity and better network to accommodate the volume charge of sulfur; the mixing of $Li_{10}GeP_2S_{12}$ improved electronic/ionic conductivity and reduced interface impedance between electrode and solid electrolyte.

In addition, Zhang et al.[122] fabricated an effective cathode candidate of Se doped sulfurized polyacrylonitrile composite ($Se_{0.05}S_{0.95}$@pPAN) used in ASSLSB. In their opinion, the uniform distribution of Se at molecular level functioned as a eutectic accelerator through the Se—S bonding, which intended to boost electronic conduction and accelerated reaction kinetics at the same time. As a result, the $Se_{0.05}S_{0.95}$@pPAN cathode (1 mg cm^{-2} sulfur loading) could deliver an initial capacity of 840 mAh g^{-1} at 167.5 mA g^{-1} and maintained a high capacity retention of 81% for 150 cycles. Meanwhile, Li et al.[123] proposed a new strategy of Se–S solid solution chemistry in S-based cathodes for ASSLBs. The introduction of Se in S helped to modify the electronic/ionic conductivities and ultimately enhanced cathode utilization. Combined with $Li_{10}GeP_2S_{12}$–Li_3PS_4 solid electrolytes, the optimized SeS_2 cathode can exhibit an outstanding electrochemical performance of over 1100 mAh g^{-1} at

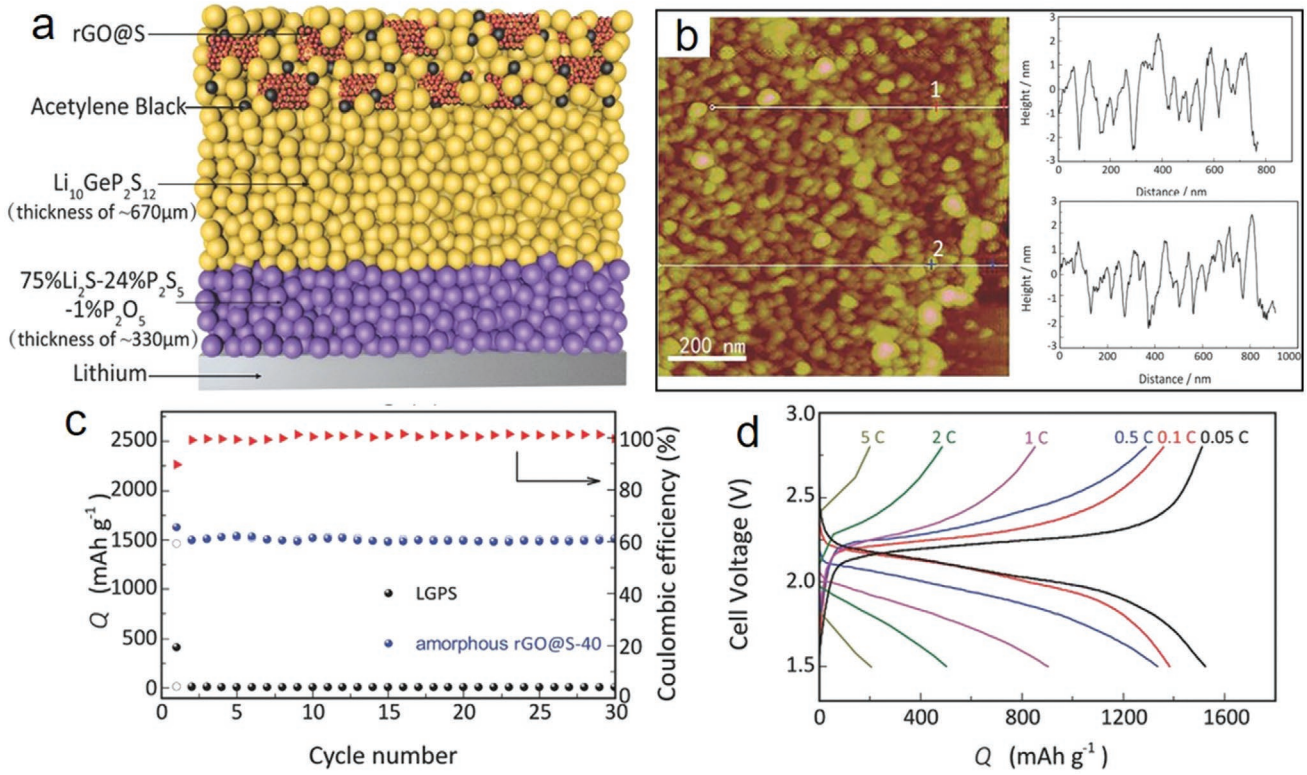

Figure 14. a) Schematic illustration of an ASSLSB battery. b) AFM images of amorphous rGO@S composite and the height profiles at lines 1 and 2. c) Cycling performances of the amorphous rGO@S composite. d) Galvanostatic discharge–charge curves for the amorphous rGO@S composite in ASSLSB. a–d) Reproduced with permission.[120] Copyright 2017, Wiley-VCH.

50 mA g^{-1} with a stable cycling for 100 cycles. Therefore, further improvements of ionic and electronic conductivities for the S-based cathode especially maintaining their stability are crucial for a high-performance ASSLBs.

3.3.2. Li_2S

Li_2S has also been employed as the cathode for ASSLB. Highly conductive metals are generally adopted to activate the electrochemical reaction due to the high insulative of Li_2S.[124] Tatsumisago's group reported the synthesis of Li_2S–Cu composite cathode by mechanical milling crystalline Li_2S and Cu powders.[125] The ASSLSB of In/Li_2S–Cu were assembled by adopting the Li_2S–P_2S_5 as electrolyte. It was revealed that the addition of Cu and the mechanical activation improved the electrochemical performance. The morphology and structure analyses demonstrated that the milling process partially form the amorphous Li_xCuS domain. This domain is important for improving the capacity. An enhanced initial discharge capacity of 490 mAh g^{-1} can be obtained. However, the use of heavy metal will decrease the energy density. Afterward, the same group reported a higher capacity Li_2S–nanocarbon composite cathode of Li_2S and AB by ball-milling process to form Li_2S–AB composite, then, Li_2S–AB was further milled with SEs to form Li_2S–AB–SEs composite cathode. The milling process enhanced the close contact between Li_2S, AB, and SEs. The cross-sectional scanning transmission electron microscopy (STEM) and electro energy loss spectroscopy (EELS) image of Li_2S composite electrode revealed that nanocomposites with intimate contacts were obtained, forming a triple junction (**Figure 15**a). More importantly, the unique structure was retained after 10 cycles (Figure 15b). Therefore, the ASSLBs employing the composite as cathodes display not only a high initial capacity of 700 mAh g^{-1}, but also a stable cycling life (Figure 15c,d).[126] In order to improve the utilization of Li_2S and understanding of Li_2S/S conversion reaction in ASSLSBs. Hakari et al.[127] systematically compared the electrochemical performance of Li_2S that mixed with different lithium halides LiX (LiCl, LiBr, and LiI) in ASSLSBs. The 80Li_2S–20LiI composite cathode exhibited the best electrochemical performance and the highest Li_2S utilization. The battery with80Li_2S–20LiI cathode retained a reversible capacity of 980 mAh g^{-1} at 2C for 2000 cycles. The significant improvement of Li_2S utilization was attribute to the increase of electrochemical reaction sites provided by dispersed LiI rather than the enhanced ionic conductivities of Li_2S–LiX solid solutions. This work provided a new insight to improve Li_2S utilization for high performance ASSLSBs.

Lin et al. demonstrated a facile synthesis approach of core–shell structure with Li_2S as core and Li_3PS_4 as the shell. Nanosized Li_2S particles were first synthesized by a liquid reaction of S with lithium triethylborohydride in THF. Subsequently, exposure of the surface of nano Li_2S with P_2S_5 results in a core–shell structure of Li_2S@Li_3PS_4, as shown in Figure 15e. Li_3PS_4 was found can improve the ionic conductivity of the cathode to 10^{-7} S cm^{-1},

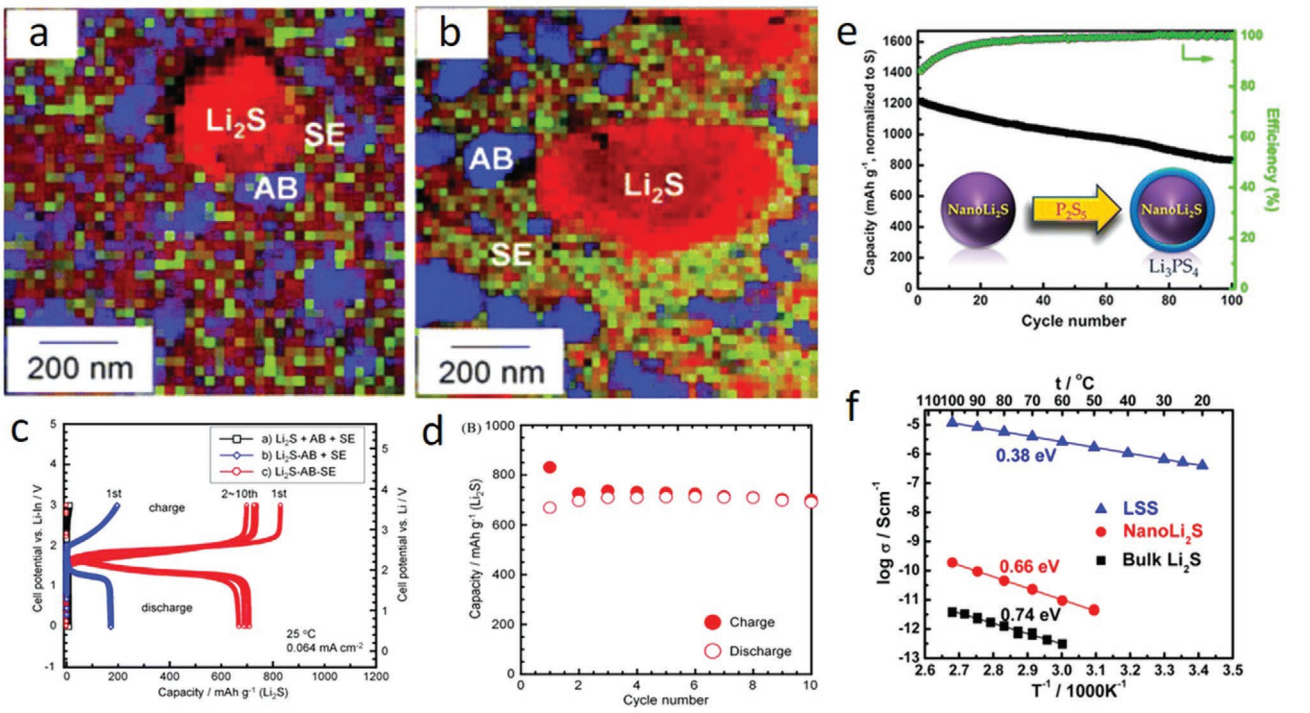

Figure 15. a,b) EELS map for Li_2S composite cathode before (a) and after 10 cycles (b) of electrochemical test. c) Charge and discharge profile of ASSLB with Li_2S/AB/SEs cathode mixtures treated differently. d) Cycle performance of the ASSLB with Li_2S–AB–SE electrode. a–d) Reproduced with permission.[126] Copyright 2012, Royal Society of Chemistry. e) Schematic of the synthesis process for core–shell structured $Li_2S@Li_3PS_4$ and the cycle performance of corresponding ASSLB. f) Temperature dependency of ionic conductivities of the bulk Li_2S, Nano Li_2S, and $Li_2S@Li_3PS_4$. e,f) Reproduced with permission.[128] Copyright 2013, American Chemical Society.

which is 6 orders of magnitude higher than that of bulk Li_2S (Figure 15f). The high ionic conductivity and reduced particle size of $Li_2S@Li_3PS_4$ delivered a high discharge capacity and cycling stability. The ASSLSB using the $Li_2S@Li_3PS_4$ as cathode delivered a large initial discharge capacity of 1216 mAh g^{-1}, and excellent capacity retention of 70% within 100 cycles.[128]

Except S and Li_2S, sulfur-rich compounds can also be used as cathode. Liang et al. first reported a series of sulfur-rich lithium polysulfidophosphates worked as the cathodes for the ASSLBs with long cyclic life.[129] Reaction of sulfur with Li_3PS_4 yielded Li_3PS_{4+n}, and sulfur was directly connected to the solid electrolyte. Thus, the sulfur will maintain continuous contact with the solid electrolyte. The polysulfidophosphates possess higher ionic conductivities by 8 orders magnitude than that of Li_2S (3.0×10^{-5} S cm^{-1} at 25 °C). The high lithium ionic conductivity imparted excellent cycling performance. Specifically, the Li_3PS_{4+n} ($n = 5$) cathode in ASSLSB presents a high reversible capacity of 700 mAh g^{-1} after 300 cycles at room temperature. The better performance of the ASSLSB can be obtained with a capacity of 1200 mAh g^{-1} after 300 cycles when the operating temperature is increased to 60 °C.

3.3.3. Sulfide Cathodes

Sulfides possess high theoretical specific capacity and have similar chemical composition and chemical potential with sulfide electrolytes, the interface will not form serious space charge layer after contacting. Therefore, it is expected to obtain high energy and long life by replacing the traditional oxide cathode material with sulfide electrode material.

Conversion Sulfide Cathodes: Conversion reaction cathode experiences following reaction

$$M_aS_b + 2bLi^+ + 2be^- \rightarrow aM^0 + bLi_2S \quad (3)$$

where nano-M^0 is highly reactive and Li_2S is highly resistive. These materials can deliver a high capacity due to the utilization of multivalent redox center. However, one challenge is their large volume change and associated structural degradation. Therefore, introduction of a buffer is the commonly used strategy to ameliorate this problem. The other problem is the agglomeration of nano-M^0 with the formation of nonreactive M, leading to the loss of reversible capacity. Thus, electronic conductive materials were incorporated into the cathode to improve the reaction kinetic between M^0 and Li_2S.

Iron sulfides are the typical conversion cathode material in sulfide-electrolyte-based ASSLB due to its high specific capacity, environmental friendless and source abundant. The reduction of FeS to Fe and Li_2S with 200% volume expansion, resulting in destruction of the electrode.[130–131] Decreasing the particle size of FeS can ameliorate the stress/strain change and decrease the conduction breakage during charge/discharge process. Besides, the higher surface area of decreased particle size FeS can increase the contact at active material/electrolyte interface, leading to the improved

high-rate capability and cycling performance. Nanostructured FeS can further increase the specific surface area and simultaneous provide shorten Li^+ diffusion path, thus improving the electrochemical kinetics. Zhang et al.[132] reported ASSLB employing FeS nanosheets as cathodes, which delivered a high capacity of 550 mAh g^{-1} within 50 cycles at 0.1 A g^{-1}. Besides FeS, many metal sulfide including NiS, CoS, CuS, etc., which are based on a conversion reaction, are often used as cathodes or composite cathodes in ASSLB.[102,111–112,133–135] Aso et al.[133] prepared an ASSLB employing NiS nanoparticles with the size of about 50 nm as cathode. Electrochemical measurements showed that the nanosized NiS delivered an initial reversible capacity of 780 mAh g^{-1} at 0.13 mA cm^{-2} and a long cycle stability, indicating an excellent reversible electrochemical performance. In addition, Long et al.[111] investigated the reaction mechanism of the NiS in all solid lithium batteries through CV and ex situ XRD, depicting a reversible conversion reaction which is similar with traditional liquid batteries.

Anionic Redox Driven Chemistry Based Electrodes: The high capacity cathodes are always derived by the reversible redox process of cations and anion (nonmetallic) or even entirely through anion redox.[136] The anionic redox reactions exist in many metal phosphides and chalcogenides. Particularly, transition metal polysulfides, such as FeS_2, TiS_3, VS_4, MoS_3, etc., where the key role is the $(S–S)^{2–}/2S^{2–}$ redox reaction. When both of cations and anions take part in the redox reaction, multielectron transfer is realized, thus an enhanced capacities can be expected. Moreover, the voltage plateau of the transition metal polysulfide electrodes is around 2.0 V, which is comparable to Li–S batteries. Thus, anionic redox driven polysulfides could be considered as promising alternatives for designing advanced materials for batteries and other energy-related applications.

In pyrite FeS_2 and patronite VS_4, sulfur is present in the form of $(S–S)^{2–}$ groups with short bond lengths (about 0.2 nm). Pyrite FeS_2 exhibits four electron conversion reaction with a theoretical capacity of 894 mAh g^{-1}.[137–138] Compared with the popular Li–sulfur system, the Li–FeS_2 system is potentially safer because FeS_2 has a much higher melting point than sulfur. However, the poor electrochemical reversibility of Li–FeS_2 chemistry limited the utilization of FeS_2 in rechargeable lithium batteries. The first discharge of FeS_2 proceeded via an intermediate Li_2FeS_2 by following a reactions[138,139]

$$FeS_2 + 2Li^+ + 2e^- \rightarrow Li_2FeS_2 \quad (4)$$

$$Li_2FeS_2 + 2Li^+ + 2e^- \leftrightarrow 2Li_2S + Fe \quad (5)$$

$$2Li_2S + Fe \rightarrow Li_2FeS_2 + 2Li^+ + 2e^- \quad (6)$$

$$Li_2FeS_2 \leftrightarrow Li_{2-x}FeS_2 + xLi^+ + xe^- \quad (0.5 < x < 0.8) \quad (7)$$

$$Li_{2-x}FeS_2 \leftrightarrow FeS_y + (2-y)S + (2-x)Li^+ + (2-x)e^- \quad (8)$$

The main advantage of such processes is the high gravimetric capacity. Lee et al.[94] found that the employment of solid electrolyte can eliminate the shuttle effect and simultaneously enable the four electron reaction of FeS_2 cathode. The FeS_2 solid state battery delivered a specific capacity of 894 mAh g^{-1} due to the fully utilized of four electron storage. In addition, the battery also demonstrated much more stable cycling performance than the same material tested in a conventional carbonate electrolyte. Similarly, Wan et al.[138] found that, after employing solid electrolyte, the reversible reaction $2Li_2S + Fe \leftrightarrow FeS_y + (2–y)S + 4Li^+ + 4e^-$ was dominated after the first cycle.

Tatsumisago et al. reported that the amorphous MoS_3 (a-MoS_3) in ASSLB shows better electrochemical performance than that of the crystalline MoS_2, due to the higher electronic conductivity of a-MoS_3 with the contribution of redox reaction of additional sulfur.[140] To further understand the reaction mechanism of a-MoS_3 electrode, the group analyzed the electronic structural change of a-MoS_3 during cycling using X-ray photoelectron spectroscopy (XPS) and X-ray absorption near edge structure (XANES).[141] The results revealed that the irreversible electronic structure changes of sulfur were observed during the first discharge/charge process, and the reaction mechanism of a-MoS_3 was proposed as follows

$$\text{a-}MoS_3 + 6Li^+ + 6e^- \rightarrow \text{a-}Li_2S\ (Li_{2-x}Mo_xS) + \text{a-}Li_xMoS_2\ \text{(1st discharge process)} \quad (9)$$

$$\text{a-}Li_xMoS_3 + 5Li^+ + 5e^- \leftrightarrow \text{a-}Li_2S\ (Li_{2-x}Mo_xS) + \text{a-}Li_xMoS_2\ \text{(after the 1st discharge)} \quad (10)$$

Zhang et al.[142] also reported the employing of rGO–MoS_3 nanocomposites as cathode for ASSLBs. After the first discharge process, the MoS_3 undergo a reversible anionic redox reaction rather than a conversion reaction. As a result, the ASSLBs depicted a better electrochemical performance than traditional lithium ion batteries due to the elimination of soluble polysulfide. Similar to a-MoS_3, VS_4 also shows an irreversible structure change after the first discharge. More importantly, high sulfur content helps to increase the specific capacity, because the sulfur also participates the reaction. Zhang et al.[143] constructed ASSLB based on GO–VS_4@$Li_7P_3S_{11}$ cathodes. The electrochemical reaction mechanisms were revealed as an initial conversion reaction followed with Li-S reaction. In addition, the dispersion of metallic V nanoparticles after first discharge process which further facilitate the transfer of the electron. As a result, the resultant battery showed a discharge capacity of 611 mAh g^{-1} at 0.1 A g^{-1} after 100 cycles.

Different from MoS_3 and VS_4, TiS_3 shows a reversible structure change during cycling, following the reversible reaction a-TiS_3 + $3Li^+$ + $3e^-$ ↔ a-Li_3TiS_3. During discharge process, $S_2^{2–}$ first react with 2 mol Li^+, then, the other 1 mol Li^+ react with $S^{2–}$ to form a-Li_3TiS_3. When charging, 3 mol Li^+ were extracted from a-Li_3TiS_3 and a-TiS_3 was formed again.[136] Similarly, amorphous TiS_4 undergo a reversible charge/discharge process. Sakuda et al.[144] revealed the reaction mechanism of amorphous TiS_4 by combining advanced techniques and theoretical calculations. Their research showed that the charge/discharge process is neither pure intercalation/deintercalation nor conversion reaction mechanism, but a mixture of the two. During the charge or discharge process, the TiS_4 undergoes two distinct structural changes: 1) the formation and deformation of S–S disulfide bonds and 2) change in the coordination number of titanium.

Based on the above discussion, anion participation in the redox reactions are always observed in transition metal

polysulfides. Both cations and anions in the redox processes offers opportunities to realize higher capacities. Further research is needed to better understand the chemistry behind their properties, to design next-generation electrode materials and to overcome the challenges associated with capacity retention.

3.4. Composite Cathodes

The materials mentioned above face the problem of low electrochemical kinetics and/or large volume expansion, thus composite materials are developed to ensure the excellent electrochemical activity of the battery. Carbon matrixes are the most common materials applied to enhance the electronic conductivity as well as alleviate the volume change. Another representative method is to use transition metal sulfide to improve the reversible conversion of sulfur to lithium sulfide, such as FeS_2@S, FeS@S, P_2S_5@S, etc. Besides, all of the components in the composites can participate in redox reaction. Passerini et al.[145] constructed an ASSLSB based on FeS_2@S composite, and the resultant battery delivered a high capacity of 1200 mAh g^{-1}. The author speculated that the addition of FeS_2 could effectively alleviate the volume change and accelerate the redox reaction. Tatsumisago et al.[146] investigated the charge/discharge mechanism of P_2S_5@S composite cathode. After ball-milling, amorphous P_2S_{5+x} was obtained. Then, with the insertion of lithium, bridging sulfurs in the amorphous P_2S_{5+x} changed to nonbridging sulfur, amorphous Li_3PS_4, and Li_2S were formed ultimately. During the following charge process, amorphous P_2S_{5+x} was reformed. In this discharge-charge mechanism, the ionic conductive part and redox sulfur are dispersed at the atomic level, leading to high electrochemical activity of the ASSLSB based on P_2S_5@S composite.

4. Lithium Anodes

4.1. Challenges for Li/Electrolyte Interface

Lithium metal has always been considered as the ultimate anode for Li-ion batteries due to its lowest electrochemical potential (−3.045 V vs standard hydrogen electrode (SHE)) and the highest specific energy (3861 mAh g^{-1}),[147] but the use of liquid or polymer electrolyte cannot suppress dendrite growth successfully which possibly results in safety concerns including fires and explosions.[148] Solid electrolytes are generally believed to be the most attractive alternative to restrict dendrite growth because of its high Li^+ transference number and high mechanical strength. However, rather than suppress dendrite growth, the dendrite formation in solid electrolytes including garnet and sulfide SEs is actually demonstrated to be much easier, which is revealed be the lower critical current density than that in nonaqueous liquid electrolyte. Therefore, in order to realize the successful integration with lithium metal anodes, dendritic Li propagation inside SEs is the critical and urgent problem to be solved.

The property of the interface layer is considered of a pivotal role in the Li dendrite formation and growth in the SEs. However, due to the narrow electrochemical window of the sulfide electrolytes, the parasitic reactions between the lithium metal/solid electrolyte interface always lead to an unstable interphase layer.[149] Hence, revealing the underlying interfacial reaction details and failure mechanism are of great significance for developing the next-generation ASSLBs with enhanced energy density and safety. In this part, we intend to focus on the key issues resulted from the combination of Li metal anode and SEs. First, the multiple dilemmas including poor interfacial stability, dendrite growth, low operation current and capacity of solid state lithium metal batteries are underscored. Specific attention is paid to the intrinsic properties such as electrochemical stability, electronic conductivity and the ionic channels of the bulk SEs. Based on the primary understandings and related analysis, the most recent proposed strategies to render an efficient and safe ASSLBs are summarized.

4.1.1. Interfacial Reaction

The stable interface between Li metal and SEs is important for enhancing Li-ion diffusion thus improving the whole electrochemical performance of the ASSLBs. An ideal interface should be highly ionically conductive and electronically insulating thus preventing the unwanted electrochemical reactions.[150] However, the interfacial reactions are complicated for ASSLBs. According to the formation features of the lithium metal/SEs interface, it can be divided into three different types.[151] In the first case, the lithium metal does not react with SEs at all, a perfect 2D thermodynamically stable interface will be formed as shown in **Figure 16**a, which has not been reported yet. In the second case, parasitic side reactions will proceed once lithium metal is in contact with SEs, forming a 3D thermodynamically unstable interfaces as shown in Figure 16b due to the highly reactive lithium metal. When the resulted interface are sufficiently electronic and ionic conductive, the dendrite will steadily grow into the SEs, pierce the bulk solid electrolytes and finally lead to the cell failure, which is defined as the mixed conducting interface.[152] The construction of a protective layer on the Li metal, also known as artificial SEI, is proven to be an effective way to avoid the formation of mixed conducting interface.[153–155] As shown in the case of Figure 16c, a metastable interface can be achieved when the bypass products have poor electronic conductivity for the sluggish reaction kinetics, which is comparable to the SEI formation in the liquid electrolyte.

Generally, theoretical studies can always provide insights and help to understand the thermodynamic and kinetic reasons of the interfacial reaction. With the help of the first-principles calculations, Zhu et al.[85,156] and Han et al.[86] found that the sulfide electrolytes are not thermodynamically stable against lithium metal and can be reduced at low voltage. The voltage curves and phase equilibria of $Li_{10}GeP_2S_{12}$ after charge and discharge are calculated as shown in Figure 16d,e. The DFT calculations reveal that the main interfacial products are Li_2S, Li_3P, and $Li_{17}Ge_4$, which can be attributed to the decomposition of sulfide electrolytes.[157]

Verification of the calculated and simulated results by experimental studies is more crucial and unavoidable. Since lithium metal and sulfide electrolytes are air- and moisture-sensitive and the lithium metal/SEs interface is always buried by the

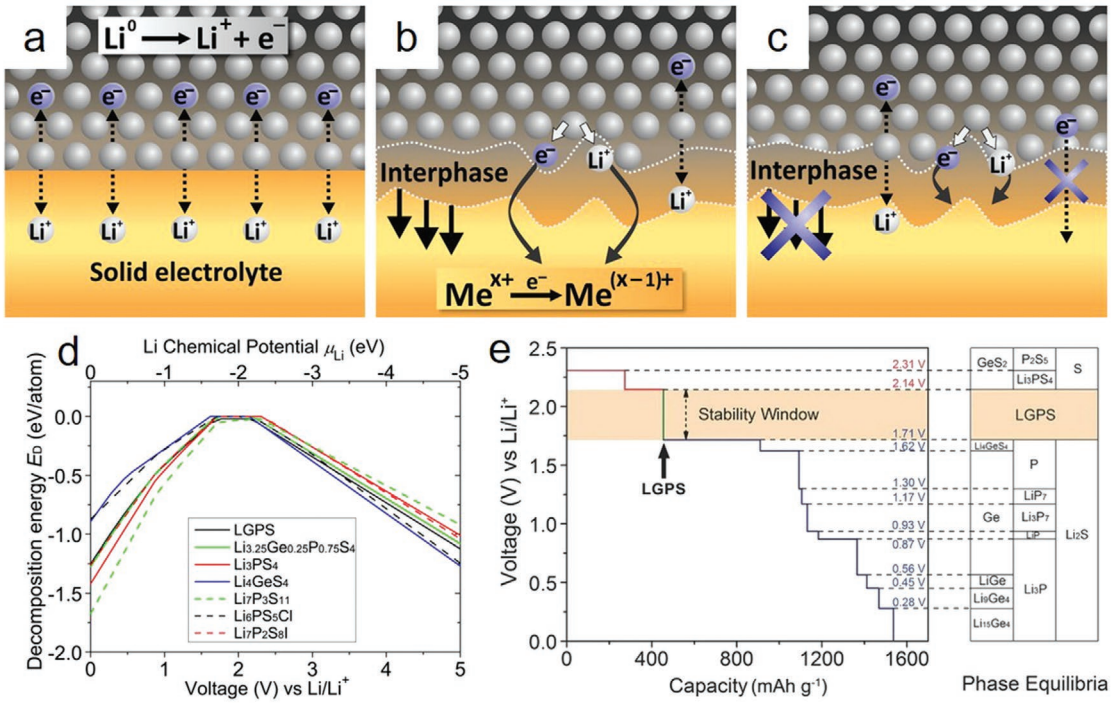

Figure 16. Schematic diagram of the types of interfaces between lithium and a solid electrolytes. a) Ideal stable interface. b) Unstable interphase. c) Metastable solid-electrolyte interphase (SEI). a–c) Reproduced with permission.[151] Copyright 2015, Elsevier. d) Decomposition energy E_D of sulfide electrolyte as a function of the applied voltage Li. Reproduced with permission.[156] Copyright 2015, American Chemical Society. e) The first-principles calculation results of the voltage profile and phase equilibria of LGPS during lithiation and delithiation. Reproduced with permission.[85] Copyright 2016, Wiley-VCH.

bulk solid phases due to the high pressure by the solid cell configuration, conventional characterization techniques such as scanning electron microscopy (SEM), transmission electron microscopy (TEM), XPS, XRD, and NMR are difficult to investigate the detailed properties. Inspired by the ionic sputtering, Janek's group[151] developed straightforward technique for investigating the formation of interphase at the surface of solid electrolytes by using an argon ion sputter gun in XPS to deposit lithium metal on the solid electrolyte surface. From the in situ XPS results, the Li_2S (around 160 eV) and Li_3P (around 126–127 eV) were formed as lithium was deposited on the $Li_7P_3S_{11}$ and all the peak intensities decrease gradually upon further deposition due to the limited probing depth. Except the formation of Li_2S and Li_3P, two additional "reduced phosphorus species" are also found by fitting the XPS spectra, which might be attributed to the formation of LiP, LiP_5 or LiP_7. Subsequently, Wenzel et al. used the same method to find a strong increase of the overall resistance of the Li/LGPS/Li cell as well as the increased thickness of SEI layer by the following reaction: $Li_{10}GeP_2S_{12} + 20Li \rightarrow 12Li_2S + 2Li_3P + Ge$.[158] Similar work has also been carried out to study long-term stability of Li_6PS_5X (X = Cl, Br, I) with Li metal.[159–160] All the three compounds can be decomposed to form an interphase composed of Li_3P, Li_2S and LiX once in contact with metallic Li. The resulted but unstable interphases lead to an increase of the interfacial resistance according to reaction of $Li_6PS_5X + 8Li \rightarrow 5Li_2S + Li_3P + LiX$ (X = Cl, Br, I). Among all the promising sulfide electrolytes, such as $Li_7P_3S_{11}$, $Li_{10}GeP_2S_{12}$, and argyrodite structure of Li_6PS_5X (X = Cl, Br, I), $Li_7P_3S_{11}$ appears to have the less side reaction with lithium metal whereas Li_6PS_5I and $Li_{10}GeP_2S_{12}$ show much higher SEI resistances.[159] As for the sulfide and thiophosphates, nearly none of them is thermostable against Li at low voltage due to their intrinsic P–S and M–S (M = Ge, Sn, Si, or Al) bonds.[84,137] The reduction potential is mainly dependent on the reduction of elemental P and Ge in the solid electrolyte, which more easily accept the unbound electron from metallic Li. Usually, a mixture products of Li_2S, Li_3P, and Li–Ge alloy is formed on the surface of $Li_{10}GeP_2S_{12}$ when the voltage drops to 0 V, which are consist with the results predicted by Ceder's group.[84,137] Although the formation of interphase has been intensively studied in recent years, the chemical composition and its evolution under battery operating conditions was not probed except by Teeter's group.[161] They revealed that the Li_2S and Li–P components at interface cause negligible polarization losses during cycling, while the formation of Li_3PO_4 phase segregation from the oxygen-contaminated LPS ($Li_3PO_xS_{4-x}$) and its subsequent growth during discharge would ruin the battery performance and cycling stability. More advanced operando characterization techniques accompanied with theoretical calculation or modeling are still urgently needed for further in-depth understanding the interfacial phase stability and reaction mechanism for the ASSLBs.

4.1.2. Lithium Dendrite

Lithium dendrite growth is one of the most important issues which has to be conquered in the rechargeable lithium metal batteries for its culprit to cell short-circuit.[162] According to

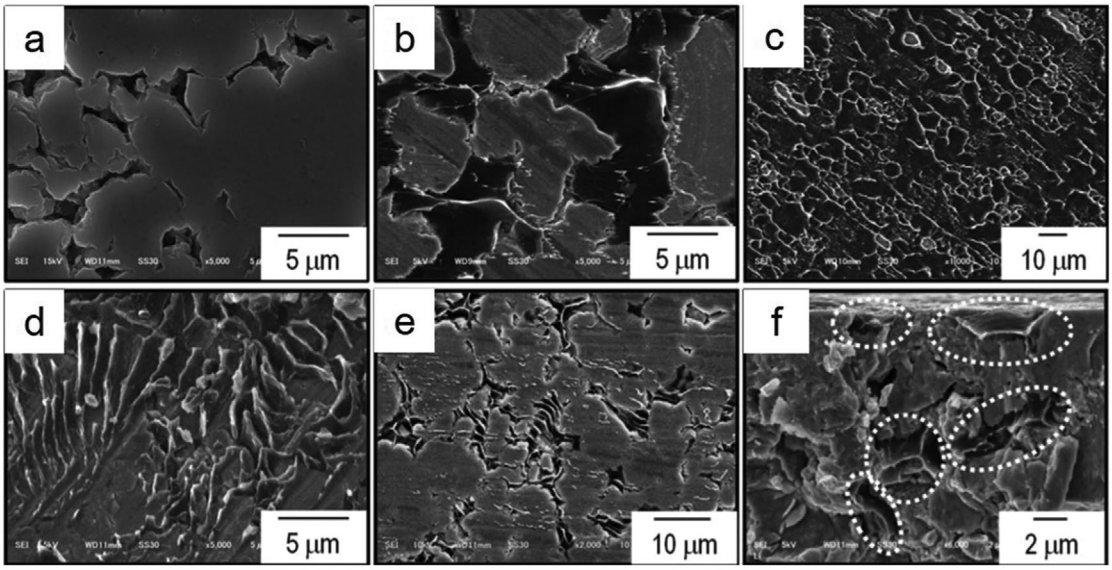

Figure 17. a–e) SEM images of the $80Li_2S{\cdot}20P_2S_5$ solid electrolyte surface: a) before cycling, and b–e) after lithium was deposited 0.05 mA cm^{-2} for 10 h (b) and 72 h (d) and at 0.5 mA cm^{-2} for 1 h (d,e). f) Cross-section of solid electrolyte at 0.5 mA cm^{-2} for 72 h. a–f) Reproduced with permission.[73] Copyright 2013, Royal Society of Chemistry.

Monroe and Newman's model, it is generally believed that the substitute of liquid electrolyte by SEs with high mechanical rigidity could effectively suppress the lithium dendrite and lead to a homogenous lithium deposition/dissolution process during cell cycling.[163] Nagao et al. found that when a small current density and areal capacity is applied, lithium can be evenly and reversibly deposited/dissolved at the lithium metal/SEs interface compared with the original one as shown in **Figure 17**a–c. While once the current density and areal capacity increase to certain values, the deposited lithium preferably nucleates and grows at the voids and grain boundaries within the SE, and further penetrates into the bulk SE, leading to the cell failure as shown in Figure 17d–f.[73] It is obvious that the inhomogeneous Li deposition mostly happens on the defects which may be aroused by the poor contact between SEs and Li metal anode or the low compaction density of internal SEs.[164–167] These defects will provide the active sites for the lithium dendrite growth. On the other hands, conductivity difference in the grain, grain boundary or the interface (SEI and electrolyte) will lead to the preferential deposition of dendrite.[168]

In order to figure out the conflicts between the theoretical model and experiment results, Chiang's group[74] investigated the Li metal penetration mechanism through four different solid electrolytes (amorphous $Li_7P_3S_{11}$, polycrystalline β-Li_3PS_4, polycrystalline, and single-crystalline $Li_6La_3ZrTaO_{12}$ garnet) and found that the nature of lithium infiltration is strongly dependent on the morphology of the electrolyte surface, in particular the defect size and density. As the current density exceeds to a critical value, the lithium penetration/infiltration occurs at the defects like surface crack and eventually results in a short circuit. Based on the results, they proposed an electro-chemomechanical model of the plating-induced lithium infiltration which suggests that the crack propagation is driven by the crack-tip stresses caused by the Li-plating in pre-existing defects.[74] Wang et al.[169] proved that the good chemical compatibility of SEs and metal anode is detrimental to the battery lifetime and favoring the fast dendrite growth which is contrary to the general understanding. The spread of lithium dendrite is highly correlated to the ionic and electronic conductivities of the interphases. More recently, Han et al.[76] conducted an operando neutron depth profile (NDP) measurement on the Li_3PS_4 solid electrolyte so as to get a real-time visualization of lithium dendrite growth. The results suggest that lithium dendrites nucleate and grow directly inside Li_3PS_4 attributed to its high electronic conductivity. Thus, how to design an elastic, scalable, and robust lithium metal/SEs interface with low electronic conductivity, high ionic conductivity, and chemical stability is necessary to alleviate the Li dendritic formation for ASSLBs with a long cycling life.

4.2. Designing Strategies for Anode/Electrolyte Interface

4.2.1. Electrolyte Optimization

Based on the discussion above, it can be concluded that the key challenge at lithium metal/SEs interface originates from the low chemical stability of sulfur-based electrolytes themselves due to the intrinsically weak P—S bonding. Therefore, tremendous works have been done to regulate the composition of solid electrolytes by doping or incorporation with other lithium compounds so as to enlarge their thermodynamic stability and electrochemical window but without lowering the high ionic conductivities.

One of the most frequently method used is replacing S^{2-} with O^{2-} due to the stronger and shorter P—O bonding. Based on first-principles, DFT and quasi-empirical bond-valence calculations, the O atom doping in β-Li_3PS_4 structure not only restrains the formation of a Li_2S-like buffer layer but also creates a new path with lower energy barrier for vacancies and Li ions at b and d sites, respectively, as shown in **Figure 18**a–c.[170]

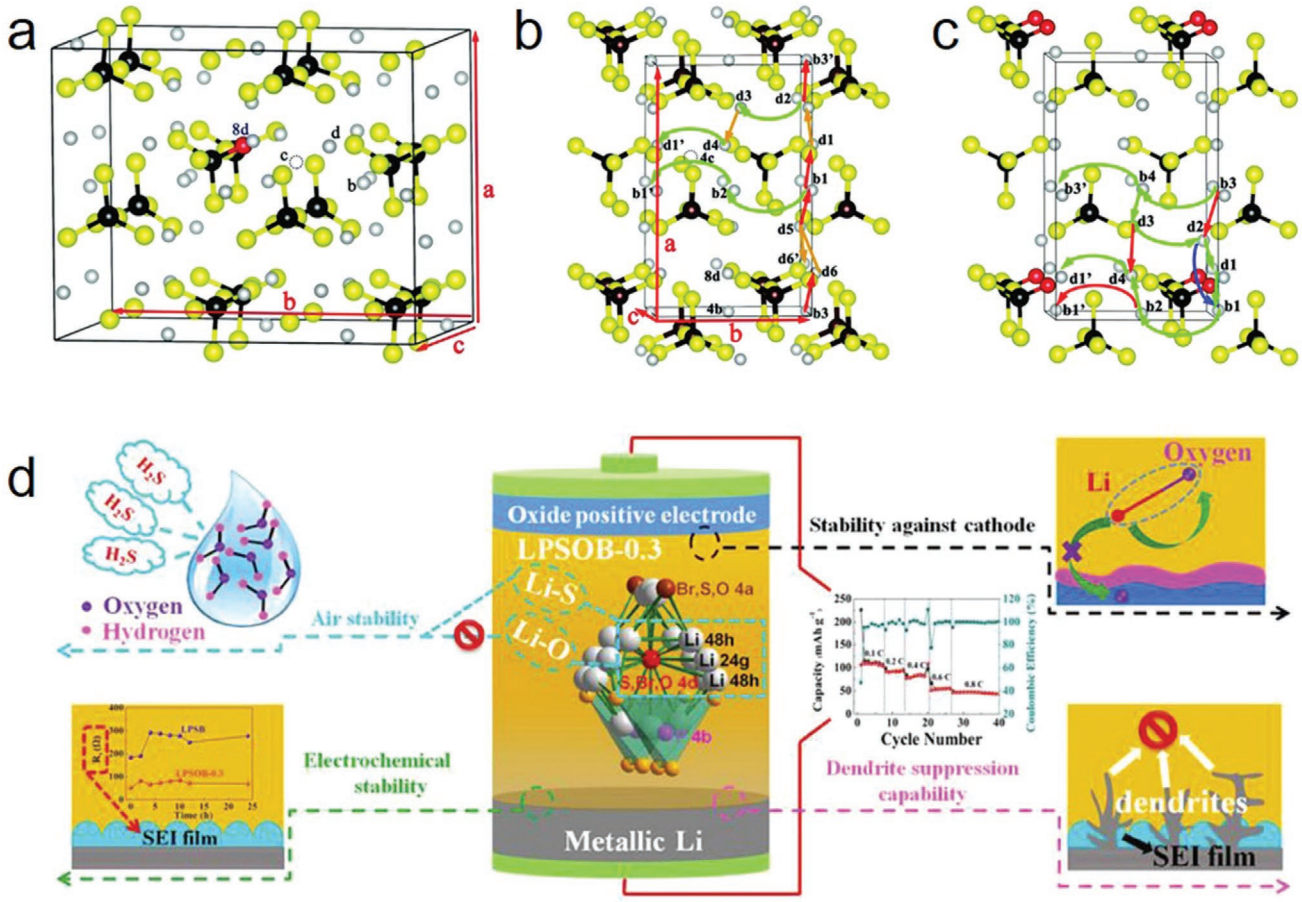

Figure 18. a) Crystal structure of β-Li_3PS_4 and the preferential substitution site when one S is replaced by O atom. b) The diffusion channels of Li-ion inβ-Li_3PS_4. green (easy), orange (moderate), red (hard). c) The migration paths calculated for $Li_3PS_{3.75}O_{0.25}$. The energy barriers presented (>0.3 eV, red line; <0.2 eV, green line). The one-step path is labeled by blue line. a–c) Reproduced with permission.[170] Copyright 2016, Royal Society of Chemistry. d) The illustration of O-doped Li_6PS_5Br argyrodite. Reproduction with permission.[171] Copyright 2019, Elsevier.

Sun et al.[172] investigated a series of $Li_{10}GeP_2S_{12-x}O_x$ with various O content and confirmed the preferential substitutability of O in the PS_4 tetrahedral. Electrochemical evaluations also demonstrated that the ASSLB using Li metal anode and $Li_{10}GeP_2S_{12-x}O_x$ of partial sulfur substitute by oxygen showed reversible capacities exceeding 100 mAh g^{-1} and better cycling performance compared to the ones with $Li_{10}GeP_2S_{12}$. Different from $Li_{10}GeP_2S_{12}$, the O atoms replace the S atoms at free S^{2-} sites rather than at the PS_4 tetrahedra in argyrodite $Li_6PS_{5-x}O_xBr$.[171] Remarkably, the O-doped solid electrolyte exhibited comprehensively enhanced properties in Figure 18d, including superior dendrite suppression capability and excellent stability against lithium reduction.

Besides single atom doping, a bunch of oxides like P_2O_5,[55] Sb_2O_5,[173] ZnO,[174] lithium halides (LiCl, LiBr, and LiI)[72,175], lithium phosphates (Li_3PO_4)[176] and others[177–178] have also been used to incorporate with SEs to enhance the structural stability and suppress the lithium dendrite growth. Although the modified electrolytes exhibit improvements of the battery performance, the parasitic interfacial reactions and lithium dendrite formation seem cannot be totally prevented during long cycling and will lead to a poor cycle life and rate capabilities.

4.2.2. Insertion of Artificial SEI

Besides electrolyte optimization, insertion of an artificial SEI will be another wise option to prevent the direct contact and undesirable side reactions of active lithium metal anode with solid electrolytes.[179] A lot of trials have been performed and inspiring achievements have been realized by the using of different chemical or physical methodologies. Ogawa et al.[180] inserted a 20 nm thick Si thin film between the lithium metal anode and Li_2S–P_2S_5 solid electrolytes and found that the cycle life was largely extended with a capacity retention of 80% after 500 cycles due to the strongly reduced reduction ability of the Li–Si interfacial layer. Similarly, other metal thin films to form alloy with metallic Li such as Au,[181–182] Al,[180] Sn,[180] and In[183] were also tested as a protective layer at the anode/electrolyte interface, which have been proven of considerable improvements especially in terms of guiding a homogenous lithium deposition and dissolution on the lithium anode during cycling. Zhang et al.[184] designed an ingenious protective layer for circumventing the intrinsic chemical stability issues of $L_{10}GP_2S_{12}$ with Li metal. The results show that a homogeneous LiH_2PO_4 protective layer between $L_{10}GP_2S_{12}$ electrolyte and Li anode can

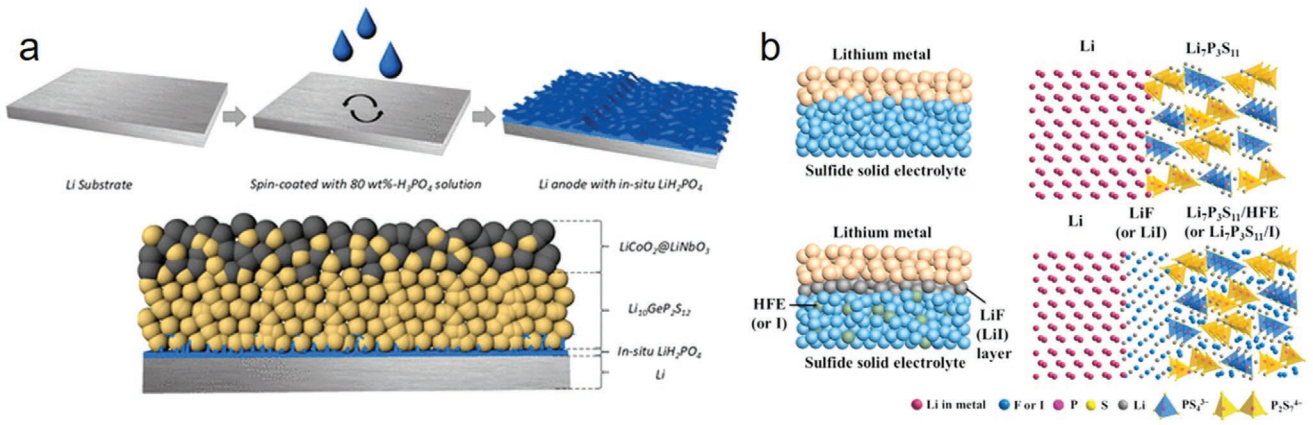

Figure 19. a) Schematic of the synthesis of in situ LiH_2PO_4 protective layer and the $LiCoO_2$/LGPS/LiH_2PO_4–Li ASSLB with optimized structure. Reproduced with permission.[184] Copyright 2018, American Chemical Society. b) Schematic diagrams of Li/$Li_7P_3S_{11}$ interface and modified interface with a uniform thin LiF (or LiI) interphase layer and HFE (or I solution) infiltrated sulfide electrolyte. Reproduced with permission.[179] Copyright 2018, Elsevier.

be in situ formed via a manipulated reaction of H_3PO_4 with Li metal in THF solution (**Figure 19**a). This approach is not only in favor of increasing the intimate contact of protective layer with the Li anode, suppressing the extension of mixed ionic-electronic reactants to the inner of $L_{10}GP_2S_{12}$, but also benefits for improving the sluggish reactions at the interface. Consequently, the symmetric Li/Li cell with $L_{10}GP_2S_{12}$ as electrolyte shows stable polarization voltage for 950 h at 0.1 mA cm^{-2}.

The LiF as the main SEI composition has been reported to effectively prevent the Li dendrite formation due to its low electronic conductivity and high interfacial energy.[185] Recently, Fan et al.[186,187] reported a high F content in SEI of Li metal anode can be achieved by increasing the Li bis(fluorosulfonyl) imide (LiFSI) concentration in carbonate-based liquid electrolyte. Such F-rich SEI not only suppressed Li dendrite formation, but also improved the Li plating/stripping Coulombic efficiency up to 99.3%. Meanwhile, they adopted an all-fluorinated electrolytes which is consisted of 1 M lithium hexafluorophosphate ($LiPF_6$) in a mixture of fluoroethylene carbonate/3,3,3-fluoroethylmethyl carbonate/1,1,2,2-tetrafluoroethyl-2′,2′,2′-trifluoroethyl ether (FEC:FEMC:HFE, 2:6:2 by weight) to lower the cost of high concentration of the Li-salts with the same effect of LiF protection. Subsequently, they also designed an in-situ LiF-rich SEI by infiltrating a drop of high concentrated 6 M LiFSI dimethoxyethane (DME) between the Li metal anode and Li_3PS_4 electrolyte, which was then dried under vacuum at high temperature to remove DME solvent.[187] Due to the reaction of the LiFSI with the Li metal, the LiF-rich SEI is successfully obtained to inhibit the penetration of Li dendrites into Li_3PS_4 electrolytes and further block the side reactions between the SEs and Li. Compared with bare Li anode, the Li metal with LiF-rich SEI improves the critical current density of Li_3PS_4 from 0.7 to 2 mA cm^{-2} and the Coulombic efficiency from 88% to 98%. As discussed above, if the solid electrolyte is a low electronic insulator and high ionic conductor, the Li dendritic formation can be avoided. However, most sulfide electrolytes are not thermodynamically stable to Li metal which form the electronic conductive SEI and lead to the continuous reaction between Li metal and the solid electrolytes. Therefore, the in situ formation of the LiF layer on Li metal surface will effectively block its side reactions with the solid electrolytes, which further suppressed the dendrite formation due to the high interfacial energy and high bulk modulus of LiF to metallic Li. Xu et al. also intended to suppress the Li dendrite by constructing a layer composed of LiF or LiI at the interface between Li anode and electrolytes.[179] As schemed in Figure 19b, both the LiF and LiI interlayer shows a capability to suppress the Li dendrite. Furthermore, the Li dendrites will be consumed by the coated HFE inside the bulk electrolyte even if the Li dendrite penetrate LiF/LiI interlayer, thus the destroy effect brought by Li dendrite can be avoided. For the galvanostatic discharge/charge of cells, the LiF coated cell still maintained a stable and low overpotential for 200 cycles under a current density of 0.5 mA cm^{-2}, showing excellent interface stability and efficient dendrite suppression.

In addition to the inorganic layer, inorganic–organic hybrid interlayer at the lithium/solid electrolyte interface is also adopted to block the interfacial electron transfer and suppress the lithium dendrites formation.[188] The lithium metal anode protected by succinonitrile-based plastic crystal electrolyte enables a high capacity retentions for both ASSLBs coupled with $LiFePO_4$ or polyacrylonitrile-sulfur (PAN-S) composites cathodes.[189–190] Moreover, it has been reported that the pretreatment of Li metal surface by N_2,[191] H_3PO_4,[184] and incorporation with a small amount of LiTFSI/Pyr13TFSI ionic liquid[192] also help to prolong the lifespan of the sulfide-electrolyte-based ASSLBs.

4.2.3. Lithium Alloys (LiAl, LiSi, LiSn, LiIn, LiAl)

Instead of lithium metal, In is currently used as a potential anode for ASSLBs with sulfur-based electrolytes in order to avoid the unnecessary interfacial reaction due to the constant and reversible Li_xIn alloy reaction at high voltage (≈0.62 V) when the Li content is less than 0.9.[193] However, this will lead to a much decreased discharging platform. Besides, the mass density of In is ten times larger than Li, the energy density decreases dramatically with the application of In anode, which strongly lowers the competitive edge of the ASSLBs compared to the traditional Li-ion batteries. Also, under the

help of in operando synchrotron X-ray tomography and energy dispersive diffraction, Sun et al.[194] observed that voids and cavities were continuously generated at the interface between LiIn and thio-LISION $Li_{10}SnP_2S_{12}$ electrolyte due to the inhomogeneous lithium deposition/dissolution during cycling, which resulted in a loss of interface integrity and undoubtedly a electrochemical performance decay. Therefore, searching other lithium alloy anode with much lower density and good chemical stability against sulfur-based SEs is more realistic. A series of Li–M alloys were investigated by Kanno's group in the past decades, such as LiAl foil,[195] LiAl powder,[196] LiSi, and LiSn foil.[197]

5. Structure Design in ASSLBs

5.1. Composite Design of the Sulfide Electrolyte

5.1.1. Bilayer Inorganic Composite Electrolyte

Due to the ultrahigh active nature of Li metal with low electrochemical potential, most of the sulfide solid-state electrolytes will be reduced when in direct contact with the pure lithium metal.[156,82] An ideal interface should obtain high electronic resistivity and high Li-ionic conductivity, which is in favor of the rapid diffusion of Li ion and complete inhabitation of side reaction between Li metal and SEs. Unfortunately, most of the final reductions product of SEs are mixed-conductive, which means electron can still transfer for the continuous reaction. Especially for those highly conductive ternary SEs (Li_2S-M_xS_y-P_2S_5) with high valence ions (including Al^{3+}, Si^{4+}, Ge^{4+}, and Sn^{4+}), the formed electronically conductive Li alloy at 0 V is confirmed both by theory calculations and experimental results, which will further leads to the severe instability of interphase.[87,198]

By comparison, Li_3PS_4 and its derivatives are considered of higher stability with metallic Li, which can be mainly ascribed to the formation of Li_2S-riched buffer layer. Such a resulted interface has ultralow electronic conductivity and exhibits excellent compatibility with Li metal. Therefore, Jung et al.[199] fabricated TiS_2/Li–In cells with $Li_{10}GeP_2S_{12}$/Li_3PS_4 as the bilayer solid electrolyte, of which Li_3PS_4 intends to obtain the surface layer to protect the Li–In anode. As a result, an outstanding electrochemical performance of ≈60 mAh g^{-1} at 20C was expected in their full cell with the optimized structure.

Meanwhile, 75%Li_2S–24%P_2S_5–1%P_2O_5 electrolyte was reported by our group as a buffer layer between $Li_{10}GeP_2S_{12}$ and metallic Li anode. Such a bilayer composite electrolyte could be successfully used in various ASSLBs with different types of sulfur-based cathodes. As show in **Figure 20**, the solid full cell, employing the $Li_{10}GeP_2S_{12}$/75%Li_2S–24%P_2S_5–1%P_2O_5 bilayer electrolyte and the highly crystalline (hc) VS_2–$Li_{10}GeP_2S_{12}$–super P cathode, demonstrated an excellent long-cycling performance, which still maintained a high discharge capacity of 270.4 mAh g^{-1} at 500 mA g^{-1} after 100 cycles.[200] Besides, other ASSLBs with sulfide-metal-based nanocomposite cathodes and similar bilayer electrolyte also exhibited the outstanding capacity retention with high electrochemical stability, including Cu_2ZnSnS_4/graphene,[201] S/rGO[120] and VS_4/rGO.[143] Therefore, it is acceptable that if the reaction between Li metal and SEs is controlled by only forming a singly ionic-conducting interface. And according to the different role of each component in the full cell, it is reasonable and beneficial to design the solid electrolytes with various combinations and configurations, which needs more systemic investigations in this field.

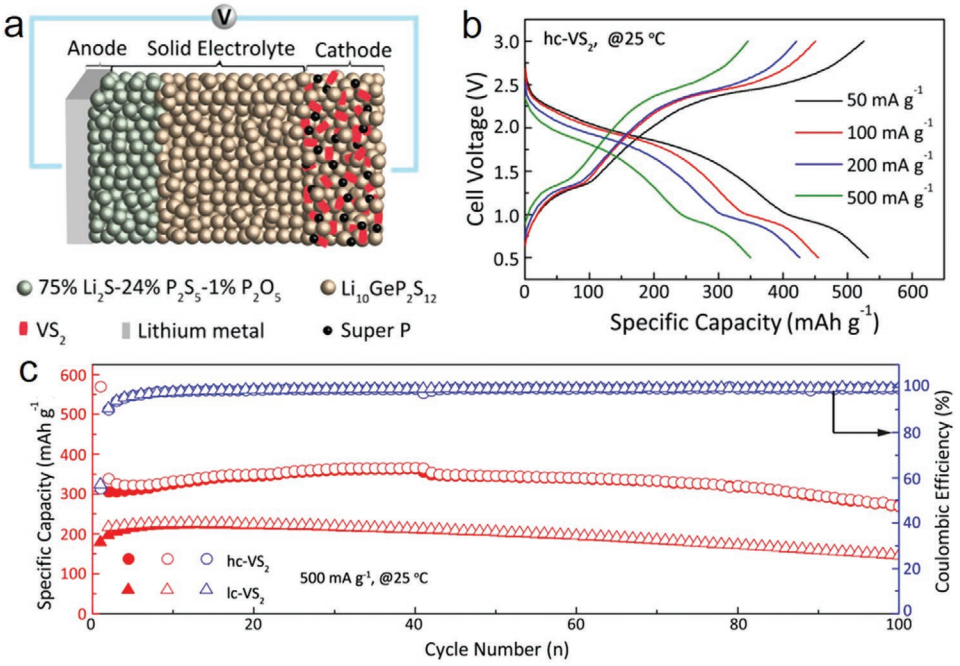

Figure 20. a) Schematic diagram of the Li/hc-VS_2 ASSLBs with 75%Li_2S–24%P_2S_5–1% P_2O_5/$Li_{10}GeP_2S_{12}$ bilayer electrolytes. b) The 20th charging–discharging profile of the batteries with hc-VS_2 electrodes at various rates and c) the cycling performance at 500 mA g^{-1}. a–c) Reproduced with permission.[200] Copyright 2018, American Chemical Society.

5.1.2. Polymer/Inorganic Composite Electrolyte

To achieve a synergetic effect of inorganic electrolyte and organic polymer, composite electrolyte is always designed to achieve a higher conductivity and proper mechanical flexibility in practical ASSLBs. Due to the thermal stability and wide electrochemical window, PEO-based polymer is frequently introduced to the inorganic electrolyte, which aims to form a close interfacial contact between electrolyte and electrode in the working battery. Cho et al.[202] fabricated a glass–polymer composite electrolytes by mixing the prepared $0.4GeS_2$–$0.3Li_2S$–0.3LiI glass and $P(EO)_8$–$LiN(CF_3SO_2)_2$ polymer. The optimal glass–polymer composite containing 13 vol% PEO delivered a high lithium-ion transference number of 0.97 with a high ionic conductivity of 8×10^{-4} s cm^{-1} at 80 °C. Our group also designed a composite electrolyte membrane with free-standing structure by the incorporation of $Li_{10}GeP_2S_{12}$ powder with PEO-based polymer.[203] Here, the $Li_{10}GeP_2S_{12}$ sulfide electrolyte acted more as the active filler in the PEO matrix and the ionic conductivity of the composite membrane containing 1% $Li_{10}GeP_2S_{12}$ reached the highest value (1.21×10^{-3} S cm^{-1} at 80 °C), nearly 80% higher than that of PEO_{18}–LiTFSI electrolyte (**Figure 21**a). $Li_{10}GeP_2S_{12}$ microparticles helped to enhance the crosslinking sites as well as suppress the plasticizing effect on their polymer electrolytes, leading to the lower glass transition temperature (T_g) of composite electrolyte. And as a single-ion conductor, $Li_{10}GeP_2S_{12}$ also provided more conducting pathways for Li ion transport, which helps to improve both ionic conductivity as well as transference number of lithium ion. Besides, we also incorporated Li_3PS_4 with PEO polymer matrix through an in situ solution preparation method.[204] Due to the excellent distribution Li_3PS_4 nanoparticles as active fillers scattering in the PEO, a considerable ionic conductivity of 8.01×10^{-4} S cm^{-1} at 60 °C was achieved when 2 vol% Li_3PS_4 was added in PEO, which enabled $LiFePO_4$/Li battery with 80.9% capacity retention after 325 cycles at 0.5C.

Other kinds of organic polymer were also added into the inorganic electrolyte to improve the flexibility as well as the conductivity of hybrid electrolytes. Hayashi et al.[205] used a terminated oligomer (1,4-butanediol) to mechanically mix $Li_7P_3S_{11}$ glasses, of which the former provided −OH group to combine with the P-S-P network in inorganic Li_2S–P_2S_5 sulfide glass to form P−O−C bonds in the hybrid materials. When the molar ratio of oligomer was increased to 2 mol%, the ionic conductivity of hybrid electrolyte could reach 9.7×10^{-5} S cm^{-1} at ambient temperature. To further enhance the compliance and adhesion of active electrode particles to the inorganic electrolyte, Villaluenga et al.[206] also reported a nonflammable hybrid electrolyte consisted of Li_3PS_4 glass and perfluoropolyether polymer. The hybrid with 23 wt% perfluoropolyether could achieve an ambient temperature conductivity close to 10^{-4} S cm^{-1} and the cationic ion transference number reaches approximately unity. Besides, its superior property of limiting lithium polysulfide dissolution was also confirmed by X-ray absorption spectroscopy, which indicated the great potential in Li–S cells. Whiteley et al.[207] also reported an in situ crosslinking process to construct a continuous network in the sulfide electrolyte ($77.5Li_2S$–$22.5P_2S_5$) by adding 20% polyimine powders, followed by heating and pressing process. Due to the excellent dispersion and connected domains of polyimine, the void spaces of the inorganic electrolyte are ideally filled, greatly enhancing the malleable property and structural stability of the composite electrolyte. As a result, the composite electrolyte membrane achieved an ultrathin thickness of only 63.7 µm (Figure 21b) as well as a high ionic conductivity of 1×10^{-4} S cm^{-1} at room temperature, nearly that of bulk electrolyte. When used in full cells with FeS_2 electrode, the hybrid electrolyte also endowed an excellent capacity retention up to 74% for 200 cycles at 0.2 C (Figure 21c). However, these synergetic designs are all at the expense of the decreased ionic conductivity of the inorganic solid electrolyte. How to effectively improve the ionic conductivity of polymer/inorganic composite electrolyte to greater than 10^{-3} S cm^{-1} and ensure its application in larger scale is still a huge and unresolved problem for researchers.

5.2. High Cell-Lever Energy Density in ASSLBs

All active and inactive components (active electrode material, electrolytes, electrode additives, and so on) should take into account when estimating the practical energy densities of a battery. The energy densities of typical sulfide-based ASSLBs based on the weights of cathode, both anode and cathode, and full cell are summarized in **Table 3**. Generally, most ASSLBs demonstrated a promising energy density larger than 300 Wh kg^{-1} based on the weight of the sulfur-based cathode. If the mass of anode has been taken into account, then the energy density of ASSLBs with Li-alloy

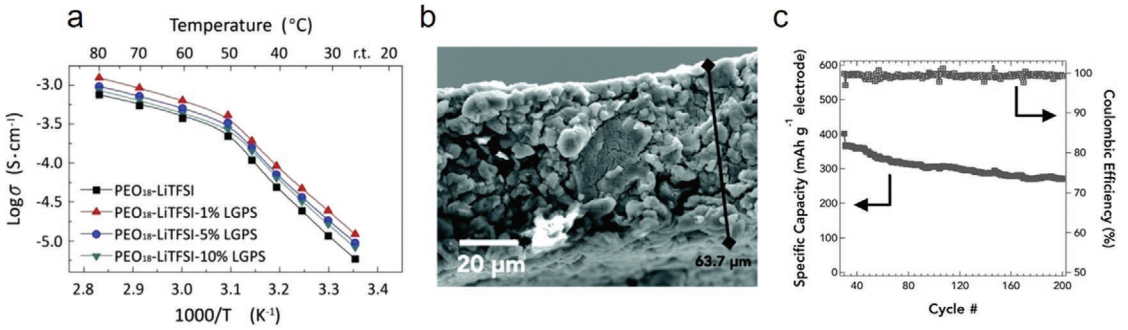

Figure 21. a) Arrhenius conductivity plots of the composite electrolyte with different LGPS contents. Reproduced with permission.[203] Copyright 2016, Elsevier. b) The cross-sectional SEM image of 7.5 mg cm^{-2} sulfide electrolyte membrane with polyimine matrix and c) long-term cycling of the FeS_2-based full cells at 0.2C. b,c) Reproduced with permission.[207] Copyright 2015, Wiley-VCH.

Table 3. Energy densities of different all-solid-state lithium batteries.

Active material cathode/active material [mg mg^{-1}]	Electrolyte [mg]	Anode [mg]	Capacity[a] [mAh g^{-1}]	Average voltage[a] [V]	Current density [mA cm^{-2}]	Energy density[b] [Wh kg^{-1}]			Ref.
						Cathode level	Cathode + anode level	Full-cell level	
S (18.4/4.6)	$Li_{10}GeP_2S_{12}$ (100)	Li–In (60.1)	1012.9	1.4	0.21	354.5	83.1	36.5	[209]
S (8/2.7)	Li_6PS_5Cl (80)	Li–In (48.3)	1081	1.3	0.568	474.2	67.4	27.8	[210]
S (7.8/2.7)	Li_3PS_4·0.5LiI (100)	Li (6.1)	1070	2.0	2.28	740.7	417.5	50.7	[211]
S (7.5/3.75)	$Li_{10}GeP_2S_{12}$ (70)	Li–In (50)	1600	1.5	0.64	1200	156.7	70.5	[119]
S (12/2.4)	Li_6PS_5Cl (88)	Li–In (46.6)	1200	1.5	0.064	360	73.7	29.5	[212]
PAN-S (10/5.7)	$77.5Li_2S$–$22.5P_2S_5$ (200)	Li (5)	659	1.9	3.2	713.6	475.8	33.2	[213]
S (3.3/1)	Li_3PS_4 (100)	Li (5.1)	1400	2.0	0.025	848.5	333.3	25.8	[214]
S (5/0.75)	$Li_{3.25}Ge_{0.25}P_{0.75}S_4$ (70)	Li–Al (19.9)	1500	1.7	0.13	382.5	76.8	20.2	[215]
S (5/0.45)	$Li_{10.05}Ge_{1.05}P_{1.95}S_{12}$ (70)	Li–In (63.6)	1500	1.1	0.48	148.5	10.8	5.4	[216]
S (5/2)	Li_3PS_4 (80)	Li–In (114.1)	1200	1.1	1.3	528	22.2	13.3	[118]
S (2.75/0.33)	LGPS/$75Li_2S$·$25P_2S_5$·$1P_2O_5$ (150)	Li (3.35)	1629	2.1	0.13	410.5	185.1	7.2	[120]
S (4.4/1)	$80Li_2S$–$20P_2S_5$ (–)	Li (–)	400	2.1	0.11	190.9	–	–	[217]
S (15/3)	Li_6PS_5Br (100)	Li–In (–)	1400	1.8	0.64	504	–	–	[218]
S (5/0.75)	$Li_{3.25}Ge_{0.25}P_{0.75}S_4$ (70)	Li–Al (–)	1600	1.5	0.13	360	–	–	[117]
S (11.2/3.37)	Li_3PS_4 (–)	$Li_{4.4}Si$ (15.0)	1300	1.5	0.1	586.7	250.8	–	[219]
S (5/1.25)	$Li_{3.25}Ge_{0.25}P_{0.75}S_4$ (70)	Li–In (61.6)	1200	1.5	0.13	450	33.8	16.9	[220]
S (1.4/0.7)	Li_3PS_4 (300)	Li–In (88.2)	1370	1.8	0.15	1233	19.2	4.44	[53]
S (11.2/3.37)	Li_3PS_4 (–)	$Li_{4.4}Si$ (15.0)	1270	1.5	0.1	573	245	–	[221]
Li_3PS_{4+5} (0.8/0.48)	Li_3PS_4 (120)	Li (3.6)	1200	2	0.015	1440	261.8	9.4	[129]
Li_2S (12/4.8)	Li_6PS_5Cl (88)	In (114)	600	1.6	0.064	384	36.6	21	[48]
Li_2S (12/4.8)	Li_6PS_5Br (88)	In (114)	500	1.8	0.064	360	34.3	20	[222]
Li_2S (10/2.5)	$80Li_2S$–$20P_2S_5$ (80)	In (57.38)	830	1.5	0.064	311.3	50.7	21.1	[126]
Li_2S (16.3/6)	Li_3PS_4 (12)	Li (1.88)	912.4	2.1	0.64	705.3	632.4	370.6	[223]
Li_2S (10/2.5)	$75Li_2S$–$25P_2S_5$ (80)	In (46)	600	1.5	0.064	225	40.2	16.5	[224]
Li_2S (3/1.2)	$75Li_2S$–$25P_2S_5$ (80)	Li–In (182.6)	1100	1.8	1.28	792	12.8	8.9	[127]
FeS_2+S (22.2/6.7)	$65Li_3PS_4$–35LiI (300)	Li (1.81)	710	2.1	0.083	450	416.1	30.8	[145]
NiS (10/4.5)	LGPS/$70Li_2S$·$29P_2S_5$·$1P_2O_5$ (150)	Li (4.19)	670	1.5	0.59	452.3	318.7	28.5	[111]
MoS_3 (2/0.9)	LGPS/$70Li_2S$·$29P_2S_5$·$1P_2O_5$ (150)	Li (3.35)	646	1.4	0.13	360	163.0	6.4	[142]
Co_9S_8@$Li_7P_3S_{11}$ (2.75/1.1)	LGPS/$70Li_2S$·$29P_2S_5$·$1P_2O_5$ (150)	Li (3.35)	633	1.5	0.38	380	171.2	6.7	[62]
TiS_2 (5/2.5)	Li_3PS_4 (150)	Li–In (100)	837	2.1	0.16	879	41.9	17.2	[106]

[a] Not all data were available as number values in the respective references. Data were extracted from figures in the respective references; [b] Energy density is calculated by initial discharge capacity multiplied by average discharge voltage.

anode decreases to less than 200 Wh kg^{-1} while that of ASSLBs with pure Li anode still maintains higher than 200 Wh kg^{-1}, revealing the importance of using pure Li metal anode in ASSLBs. Moreover, many of the reported ASSLBs use thick solid electrolytes (more than 0.5 or even 1.0 mm). As a result, the cell-level energy of ASSLBs is still not high which highlights the importance of reducing electrolyte thickness in achieving the high energy density. Up to now, several research works have been paid to the preparation of thin sulfide electrolyte. Whiteley et al.[207] reduced the thickness of solid electrolyte membrane to 64 µm through the strategy of solid electrolyte-in-polymer matrix as mentioned above. Recently, Hood et al.[208] developed a new approach to fabricate ultrathin β-Li_3PS_4 solid electrolyte membrane based on two main steps. First, a solvent exchange and solution-based exfoliation process was applied to obtain shape-controlled nanoplates of Li_3PS_4·2ACN with a unique tiled assembly property. Then a warm pressing at 200 °C of 200 MPa was carried out to promote the decomposition of Li_3PS_4·2ACN to β-Li_3PS_4 and further fusion of the solid electrolyte building blocks. Besides, they found the thickness of the β-Li_3PS_4 films could be readily tailored by tuning the concentration of the Li_3PS_4·2ACN nanoscale building blocks in ACN. As shown in **Figure 22**a–f, ultrathin membranes ranging from 0.4 to 35 µm were obtained when tuning the concentration from 0.1 to 0.8 M, which also showed desirable ionic

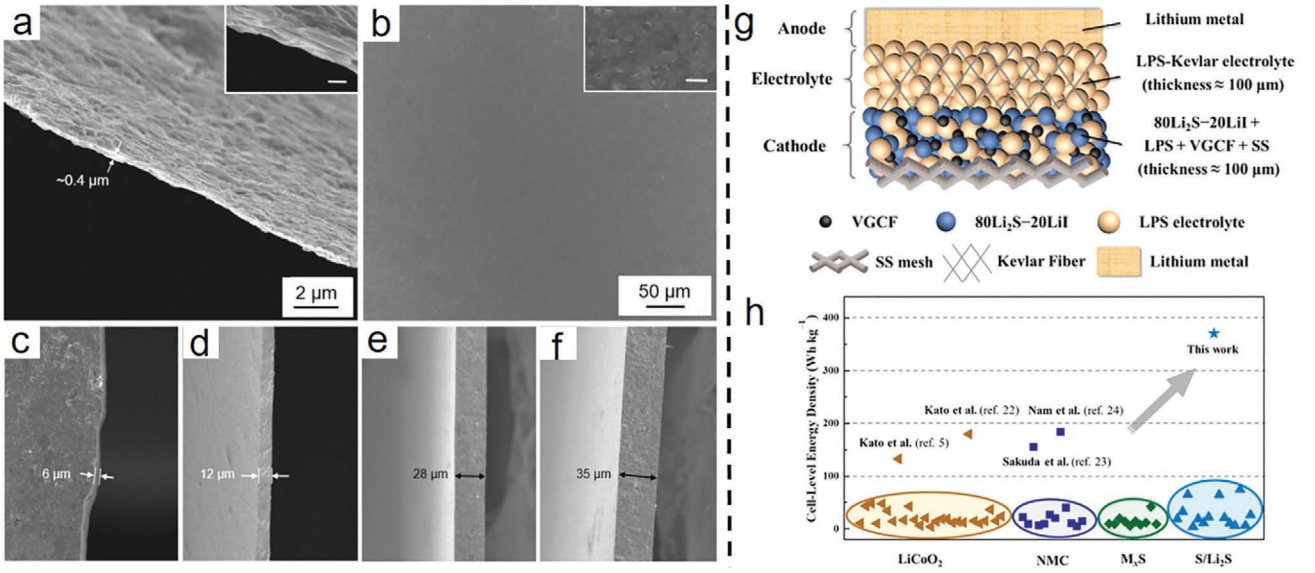

Figure 22. a–f) SEM images of the β-Li_3PS_4 ultrathin film with a thickness varying from 0.4 to 35 μm. a–f) Reproduced with permission.[208] Copyright 2018, Wiley VCH. g) Schematic illustration of cathode-supported Li–Li_2S solid cell and h) the comparison of cell-based energy density of the reported cells with sulfide electrolytes. g,h) Reproduced with permission.[223] Copyright 2019, American Chemical Society.

conductivity and necessary compatibility with metallic lithium anodes. However, there is lack of full cell performance about the sub-micrometer β-Li_3PS_4 membranes, which may need more comprehensive research in the near future.

Another huge challenge for the practical application of ASSLBs is to further increase the cathode thickness, especially under the employment of thin electrolyte pellet. Recently, Xu et al. tried to build the solid cell from the first step of constructing Li_2S cathode with a stainless steel (SS) framework, which was prepared by a dry grinding and rolling process.[223] Then a thin Kevlar nonwoven-supported Li_3PS_4 glass solid electrolyte of around 100 μm and the bare 45 μm Li foil were subsequently stacked under cold pressing to obtain the three-layered full cell (Figure 22g). Due to the reduced thickness of Li_3PS_4 electrolyte as well as the much-improved mechanical integrity of Li_2S cathode by SS mesh, the Li–Li_2S cell performed a stable discharge capacity of 949.9 mAh g^{-1} at 0.05 C with the Li_2S loading of 2.54 mg cm^{-2}. An ultrahigh energy density of 370.6 Wh kg^{-1} was also achieved when increasing the Li_2S loading to 7.64 mg cm^{-2} (Figure 22h). However, such a high specific capacity is only achieved in the first cycle and gradually fades to nearly 45% after 20 cycles. Hence, more research in high-energy-density ASSLBs with long-term cycling and stable energy retention are needed in the near further.

6. Summary and Outlook

The ASSLBs are now attracting fast-growing interests, especially for their great potential to fundamentally solve the safety concern and significantly improve the energy density of a working cell. In this review, the very recent progresses in sulfur-based cathodes for ASSLSBs utilizing sulfide electrolytes and the key interfacial issues between the electrode and electrolyte are systematically reviewed and discussed. Besides, the main challenges and corresponding strategies to improve the performance of ASSLBs with sulfur-based cathodes are also proposed, which offers a meaningful guideline to promote further research in this field.

Specifically, preparation methods to fabricate different sulfide electrolytes are clearly summed up and their general physicochemical properties are also discussed in depth. More than excellent ionic conductivity, weak electronic conductivity is also desired for an ideal sulfide electrolyte, of which the latter one plays a more critical criterion to suppress dendrite formation in ASSLBs. For the practical commercialization of the sulfide electrolytes, the air-stability is another bottle-neck to break through. On the side of sulfur-based cathodes, various types of materials ranging from sulfur, lithium sulfide and metal sulfides are classified in detail. Despite their favorable compatibility with sulfide electrolyte, the unavoidable stress/strain resulted from electrochemical cycling can also lead to a severe interfacial problem. To improve the specific capacity and electrochemical cyclability, various effective ways are adopted, which mainly intend to decrease the particle size of the active materials, construct the electron/ion conducting framework, and design 3D structures to mitigate volume change. Some new strategies such as introducing catalytic sites to promote S-conversion reactions or the named "confined spaces" to accommodate the dissolved S-species are also effective to improve the performance of ASSLBs. On the side of anode, different Li–M alloy (M includes In, Ge, Si, Sn, Al, etc.) are used as the substitutes for Li metal anode, but this will result in low cell voltage and reduced capacity. ASSLBs can only show its superiority in energy density when the lithium metal anode is employed. At present, two main methodologies including artificial SEI construction of metallic lithium anode and the insertion of thin lithium alloying film are routinely used to minimize interfacial resistances. Despite Li_3PS_4 and its derivatives exhibit a relevant stability with lithium metal, the capacity

utilization and working current density of lithium metal anodes seems far from practical requirements (lager than 3 mAh cm^{-2} at 3 mA cm^{-2}). Therefore, it is still a huge challenge to solve the interfacial contact as well as dendrite formation problems of ASSLBs with sulfide electrolyte.

In summary, the ASSLB with sulfur-based cathode and sulfide electrolyte is a promising candidate for next-generation and high-energy rechargeable battery despite with many barriers to overcome. Practically, adopting a straightforward strategy, simply aiming to improve electrolyte conductivity, or electrode capacity or interface stability alone, seems could hardly make a revolutionary and complete solution of ASSLBs, which more needs combined approaches to achieve a joint modification for high-performance ASSLBs. Herein, several principles are summarized and deserve more attention in future research works regarding sulfur-based cathodes for ASSLBs with sulfide electrolytes:

1) Interfacial Li-ion diffusion mechanism. Although a lot of work has studied the ionic transport mechanism in the bulk solid electrolyte with great progress, the Li-ion diffusion behavior between the interface of electrode and electrolyte (both the electrode/SE interface and active material/SE interface in electrode) still lack in-depth understanding. We expect that advanced operando characterization techniques including solid-state NMR, NDP, X-ray diffraction, photoelectron spectroscopy, and in situ electrochemical techniques should be properly combined to study the fundamental Li-ion diffusion mechanism and reveal interfacial structure change in ASSLBs, which will provide more pertinent suggestions to address the challenging problems.
2) Exploration of new solid electrolyte. For sulfide electrolytes, some of them have shown their superiority in high ionic conductivity. However, their other properties such as poor electrochemical stability, sensitivity to ambient atmosphere, machinability, and flexibility in large scale greatly limits the practical applications. Theoretical calculation and simulation are an important tool to give brilliant instructions to design new sulfide electrolyte by predicting physicochemical properties and compatibility with active materials in advance, which will vastly accelerate the speed of boosting the research progress of ASSLBs.
3) Improving current density and specific areal capacity. The current density and capacity adopted (usually less than 1.0 mA cm^{-2} of 1.0 mAh cm^{-2}) in ASSLBs so far can hardly meet the practical requirements of 3.0 mA cm^{-2} and 3.0 mAh cm^{-2}. To apply the thick cathode with high active material loading is also desirable to ensure the energy density at full cell level. A smart electrode configuration design with perfect ionic/electronic transport is necessary in this regard. How to host active electrode materials in a 3D porous scaffold with excellent ionic and ionic conductivity and maintain the structure stability during cycling is a tough problem but worth of consideration.
4) Dendrite-free Li metal anode. In spite of the conventional opinion of dendrites can be prevented by SEs with high mechanical strength, the dendrite formation inside sulfide electrolyte is an accepted phenomenon by forefront research. Several different reasons are attributed to the dendrite growth, including low relative density of SEs, pre-existence of grain boundaries and defects, accumulated voids formed at the interface due to critical current density on stripping, and our recent finding of the intrinsically high electronic conductivity of SEs. Although it can hardly reconcile all these inconsistencies, we can conclude a joint modification may be a better choice to achieve a dendrite-free anode in ASSLBs. To achieve a high-density SEs pellet, new strategy of hot-press process should also be carried out for future research. Meanwhile, stable interface construction between Li metal and sulfide electrolyte is essential. Not only ensuring the imitate contact, the artificial interface should better possess a high interfacial energy (such as LiF-rich SEI) with ultralow electronic conductivity, which can help to regulate the lateral growth of deposited Li metal below the interface. A self-healing property is better preferred to reduce the interfacial impedance. Besides, investigations of new doping methods with new dopant materials are indispensable for further decreasing the electronic conductivity but not restraining lithium ion channels of SEs.
5) Reducing the electrolyte thickness. The pellets of sulfide electrolyte are usually much thicker than the separator (about 10 μm thick) used in conventional LIBs with liquid organic electrolyte. More efforts are required to fabricate a thin SEs in a large-scale and low-cost process. Due to the easy fracture of thin SEs during cell fabrication, one main intractable problem is to deal with the mechanical fragility. The combination of sulfide electrolytes with polymer (including solid polymer electrolyte and polymer binder) seems to be a good option, which is of vital importance to endow solid electrolytes with acceptable flexibility. However, the mixed polymer will normally lead a reduced conductivity by hampering the ionic conduction between SE particles. And the introduction of a second phase also generates other interfacial contact, which definitely have impacts on electrochemical performance of the working cell. An appropriate balance between polymer and sulfide electrolyte can only be achieved through many trial and errors.
6) Structure design of full cell. An efficient cell system requires a compatibility between various components of cathode, electrolyte, anode, and so forth. For various sulfide electrolytes, their compatibility with various sulfur-based cathodes and Li alloy or Li metal anodes also exist difference predicatively due to the specifically physicochemical properties of electrode and electrolyte materials. It is easy to obtain a composite cathode layer by mixing active material, SEs and conducting carbon together. While an interconnected electronic/ionic network with high stability during cycling is hard to realize by the simple mixing. A high compactness is necessary to avoid the generation of voids inside the composite, which need optimization of composition proportions and new strategy for mixing. Using solid electrolytes with bilayer structure to mitigate the instability with the metallic Li is an effective method, which requires more attention to understand chemical mechanism and material evolution for controllably and efficiently releasing the energy. Therefore, it is imperative to explore new techniques to design the battery structure to achieve an overall performance especially combining the existing fabrication technologies and processes, which plays an important role to promote the practical application of ASSLBs.

Acknowledgements

J.W. and S.L. contributed equally to this work. The work was supported by the National Key R&D Program of China (Grant no. 2018YFB0905400), the National Natural Science Foundation of China (Grant no. 51872303, U1964205), Zhejiang Provincial Natural Science Foundation of China (Grant no. LD18E020004, LY18E020018), and Youth Innovation Promotion Association CAS (2017342).

Conflict of Interest

The authors declare no conflict of interest.

Keywords

all-solid-state lithium batteries, sulfide electrolytes, sulfide cathodes, lithium–sulfur batteries

Received: February 19, 2020
Revised: April 10, 2020
Published online:

[1] S. Chu, A. Majumdar, *Nature* **2012**, *488*, 294.
[2] J. Lau, R. H. DeBlock, D. M. Butts, D. S. Ashby, C. S. Choi, B. S. Dunn, *Adv. Energy Mater.* **2018**, *8*, 1800933.
[3] Z. Gao, H. Sun, L. Fu, F. Ye, Y. Zhang, W. Luo, Y. Huang, *Adv. Mater.* **2018**, *30*, 1705702.
[4] L. Fan, S. Wei, S. Li, Q. Li, Y. Lu, *Adv. Energy Mater.* **2018**, *8*, 1702657.
[5] N. Kamaya, K. Homma, Y. Yamakawa, M. Hirayama, R. Kanno, M. Yonemura, T. Kamiyama, Y. Kato, S. Hama, K. Kawamoto, *Nat. Mater.* **2011**, *10*, 682.
[6] Y. Kato, S. Hori, T. Saito, K. Suzuki, M. Hirayama, A. Mitsui, M. Yonemura, H. Iba, R. Kanno, *Nat. Energy* **2016**, *1*, 16030.
[7] C. Sun, J. Liu, Y. Gong, D. P. Wilkinson, J. Zhang, *Nano Energy* **2017**, *33*, 363.
[8] J. C. Bachman, S. Muy, A. Grimaud, H.-H. Chang, N. Pour, S. F. Lux, O. Paschos, F. Maglia, S. Lupart, P. Lamp, L. Giordano, Y. Shao-Horn, *Chem. Rev.* **2016**, *116*, 140.
[9] A. Manthiram, X. Yu, S. Wang, *Nat. Rev. Mater.* **2017**, *2*, 16103.
[10] K. Kerman, A. Luntz, V. Viswanathan, Y.-M. Chiang, Z. Chen, *J. Electrochem. Soc.* **2017**, *164*, A1731.
[11] Y. Seino, T. Ota, K. Takada, A. Hayashi, M. Tatsumisago, *Energy Environ. Sci.* **2014**, *7*, 627.
[12] A. Sakuda, A. Hayashi, M. Tatsumisago, *Sci. Rep.* **2013**, *3*, 2261.
[13] F. P. McGrogan, T. Swamy, S. R. Bishop, E. Eggleton, L. Porz, X. Chen, Y. M. Chiang, K. J. Van Vliet, *Adv. Energy Mater.* **2017**, *7*, 1602011.
[14] K. Nie, Y. Hong, J. Qiu, Q. Li, X. Yu, H. Li, L. Chen, *Front. Chem.* **2018**, *6*.
[15] R. Mercier, J.-P. Malugani, B. Fahys, G. Robert, *Solid State Ionics* **1981**, *5*, 663.
[16] M. Tatsumisago, A. Hayashi, *Solid State Ionics* **2012**, *225*, 342.
[17] A. Hayashi, S. Hama, T. Minami, M. Tatsumisago, *Electrochem. Commun.* **2003**, *5*, 111.
[18] F. Mizuno, A. Hayashi, K. Tadanaga, M. Tatsumisago, *Solid State Ionics* **2006**, *177*, 2721.
[19] A. Hayashi, S. Hama, H. Morimoto, M. Tatsumisago, T. Minami, *J. Am. Ceram. Soc.* **2001**, *84*, 477.
[20] F. Mizuno, A. Hayashi, K. Tadanaga, M. Tatsumisago, *Adv. Mater.* **2005**, *17*, 918.
[21] H. Yamane, M. Shibata, Y. Shimane, T. Junke, Y. Seino, S. Adams, K. Minami, A. Hayashi, M. Tatsumisago, *Solid State Ionics* **2007**, *178*, 1163.
[22] R.-c. Xu, X.-h. Xia, S.-h. Li, S.-z. Zhang, X.-l. Wang, J.-p. Tu, *J. Mater. Chem. A* **2017**, *5*, 6310.
[23] Z. Liu, W. Fu, E. A. Payzant, X. Yu, Z. Wu, N. J. Dudney, J. Kiggans, K. Hong, A. J. Rondinone, C. Liang, *J. Am. Chem. Soc.* **2013**, *135*, 975.
[24] H. Muramatsu, A. Hayashi, T. Ohtomo, S. Hama, M. Tatsumisago, *Solid State Ionics* **2011**, *182*, 116.
[25] K. Homma, M. Yonemura, T. Kobayashi, M. Nagao, M. Hirayama, R. Kanno, *Solid State Ionics* **2011**, *182*, 53.
[26] R. Kanno, T. Hata, Y. Kawamoto, M. Irie, *Solid State Ionics* **2000**, *130*, 97.
[27] R. Kanno, M. Murayama, *J. Electrochem. Soc.* **2001**, *148*, A742.
[28] S. Nishino, T. Fujiwara, H. Yamasaki, *Phys. Rev. B* **2014**, *90*, 024303.
[29] A. Kuhn, V. Duppel, B. V. Lotsch, *Energy Environ. Sci.* **2013**, *6*, 3548.
[30] S. P. Ong, Y. Mo, W. D. Richards, L. Miara, H. S. Lee, G. Ceder, *Energy Environ. Sci.* **2013**, *6*, 148.
[31] P. Bron, S. Johansson, K. Zick, J. Schmedt auf der Günne, S. Dehnen, B. Roling, *J. Am. Chem. Soc.* **2013**, *135*, 15694.
[32] A. Kuhn, O. Gerbig, C. Zhu, F. Falkenberg, J. Maier, B. V. Lotsch, *Phys. Chem. Chem. Phys.* **2014**, *16*, 14669.
[33] J. M. Whiteley, J. H. Woo, E. Hu, K.-W. Nam, S.-H. Lee, *J. Electrochem. Soc.* **2014**, *161*, A1812.
[34] M. Kaus, H. Stöffler, M. Yavuz, T. Zinkevich, M. Knapp, H. Ehrenberg, S. Indris, *J. Phys. Chem. C* **2017**, *121*, 23370.
[35] C. Vinado, S. Wang, Y. He, X. Xiao, Y. Li, C. Wang, J. Yang, *J. Power Sources* **2018**, *396*, 824.
[36] P. Bron, S. Dehnen, B. Roling, *J. Power Sources* **2016**, *329*, 530.
[37] S. Hori, S. Taminato, K. Suzuki, M. Hirayama, Y. Kato, R. Kanno, *Acta Crystallogr., Sect. B: Struct. Sci., Cryst. Eng. Mater.* **2015**, *71*, 727.
[38] Y. Bai, Y. Zhao, W. Li, L. Meng, Y. Bai, G. Chen, *ACS Sustainable Chem. Eng.* **2019**, *7*, 12930.
[39] S. Hori, K. Suzuki, M. Hirayama, Y. Kato, R. Kanno, *Front. Energy Res.* **2016**, *4*, 38.
[40] A. Hayashi, Y. Nishio, H. Kitaura, M. Tatsumisago, *Electrochem. Commun.* **2008**, *10*, 1860.
[41] H. J. Deiseroth, S. T. Kong, H. Eckert, J. Vannahme, C. Reiner, T. Zaiss, M. Schlosser, *Angew. Chem., Int. Ed.* **2008**, *47*, 755.
[42] P. R. Rayavarapu, N. Sharma, V. K. Peterson, S. Adams, *J. Solid State Electrochem.* **2012**, *16*, 1807.
[43] S. Boulineau, M. Courty, J.-M. Tarascon, V. Viallet, *Solid State Ionics* **2012**, *221*, 1.
[44] L. Zhou, K.-H. Park, X. Sun, F. Lalère, T. Adermann, P. Hartmann, L. F. Nazar, *ACS Energy Lett.* **2019**, *4*, 265.
[45] M. A. Kraft, S. P. Culver, M. Calderon, F. Böcher, T. Krauskopf, A. Senyshyn, C. Dietrich, A. Zevalkink, J. r. Janek, W. G. Zeier, *J. Am. Chem. Soc.* **2017**, *139*, 10909.
[46] P. Adeli, J. D. Bazak, K. H. Park, I. Kochetkov, A. Huq, G. R. Goward, L. F. Nazar, *Angew. Chem., Int. Ed.* **2019**, *58*, 8681.
[47] M. A. Kraft, S. Ohno, T. Zinkevich, R. Koerver, S. P. Culver, T. Fuchs, A. Senyshyn, S. Indris, B. J. Morgan, W. G. Zeier, *J. Am. Chem. Soc.* **2018**, *140*, 16330.
[48] C. Yu, S. Ganapathy, N. J. de Klerk, I. Roslon, E. R. van Eck, A. P. Kentgens, M. Wagemaker, *J. Am. Chem. Soc.* **2016**, *138*, 11192.
[49] D. H. Kim, D. Y. Oh, K. H. Park, Y. E. Choi, Y. J. Nam, H. A. Lee, S.-M. Lee, Y. S. Jung, *Nano Lett.* **2017**, *17*, 3013.
[50] M. Chen, X. Yin, M. Reddy, S. Adams, *J. Mater. Chem. A* **2015**, *3*, 10698.
[51] N. H. H. Phuc, K. Morikawa, M. Totani, H. Muto, A. Matsuda, *Solid State Ionics* **2016**, *285*, 2.
[52] M. Tatsumisago, *Solid State Ionics* **2004**, *175*, 13.
[53] M. R. Busche, D. A. Weber, Y. Schneider, C. Dietrich, S. Wenzel, T. Leichtweiss, D. Schröder, W. Zhang, H. Weigand, D. Walter, *Chem. Mater.* **2016**, *28*, 6152.

[54] J. Trevey, J. S. Jang, Y. S. Jung, C. R. Stoldt, S.-H. Lee, *Electrochem. Commun.* **2009**, *11*, 1830.
[55] Y. Tao, S. Chen, D. Liu, G. Peng, X. Yao, X. Xu, *J. Electrochem. Soc.* **2016**, *163*, A96.
[56] K. Minami, A. Hayashi, M. Tatsumisago, *J. Am. Chem. Soc.* **2011**, *94*, 1779.
[57] S. Wang, Y. Zhang, X. Zhang, T. Liu, Y.-H. Lin, Y. Shen, L. Li, C.-W. Nan, *ACS Appl. Mater. Interfaces* **2018**, *10*, 42279.
[58] C. Yu, S. Ganapathy, J. Hageman, L. van Eijck, E. R. van Eck, L. Zhang, T. Schwietert, S. Basak, E. M. Kelder, M. Wagemaker, *ACS Appl. Mater. Interfaces* **2018**, *10*, 33296.
[59] S. Ito, M. Nakakita, Y. Aihara, T. Uehara, N. Machida, *J. Power Sources* **2014**, *271*, 342.
[60] M. Calpa, N. C. Rosero-Navarro, A. Miura, K. Tadanaga, *RSC Adv.* **2017**, *7*, 46499.
[61] R. Xu, X. Xia, Z. Yao, X. Wang, C. Gu, J. Tu, *Electrochim. Acta* **2016**, *219*, 235.
[62] X. Yao, D. Liu, C. Wang, P. Long, G. Peng, Y.-S. Hu, H. Li, L. Chen, X. Xu, *Nano Lett.* **2016**, *16*, 7148.
[63] Y. Wang, D. Lu, M. Bowden, P. Z. El Khoury, K. S. Han, Z. D. Deng, J. Xiao, J.-G. Zhang, J. Liu, *Chem. Mater.* **2018**, *30*, 990.
[64] S. Teragawa, K. Aso, K. Tadanaga, A. Hayashi, M. Tatsumisago, *J. Mater. Chem. A* **2014**, *2*, 5095.
[65] S. Yubuchi, S. Teragawa, K. Aso, K. Tadanaga, A. Hayashi, M. Tatsumisago, *J. Power Sources* **2015**, *293*, 941.
[66] S. Yubuchi, M. Uematsu, M. Deguchi, A. Hayashi, M. Tatsumisago, *ACS Appl. Energy Mater.* **2018**, *1*, 3622.
[67] S. Yubuchi, M. Uematsu, C. Hotehama, A. Sakuda, A. Hayashi, M. Tatsumisago, *J. Mater. Chem. A* **2019**, *7*, 558.
[68] Ö. U. Kudu, T. Famprikis, B. Fleutot, M.-D. Braida, T. Le Mercier, M. S. Islam, C. Masquelier, *J. Power Sources* **2018**, *407*, 31.
[69] B. R. Shin, Y. J. Nam, D. Y. Oh, D. H. Kim, J. W. Kim, Y. S. Jung, *Electrochim. Acta* **2014**, *146*, 395.
[70] N. C. Rosero-Navarro, A. Miura, K. Tadanaga, *J. Sol-Gel Sci. Technol.* **2019**, *89*, 303.
[71] S. Chida, A. Miura, N. C. Rosero-Navarro, M. Higuchi, N. H. Phuc, H. Muto, A. Matsuda, K. Tadanaga, *Ceram. Int.* **2018**, *44*, 742.
[72] F. Han, J. Yue, X. Zhu, C. Wang, *Adv. Energy Mater.* **2018**, *8*, 1703644.
[73] M. Nagao, A. Hayashi, M. Tatsumisago, T. Kanetsuku, T. Tsuda, S. Kuwabata, *Phys. Chem. Chem. Phys.* **2013**, *15*, 18600.
[74] L. Porz, T. Swamy, B. W. Sheldon, D. Rettenwander, T. Frömling, H. L. Thaman, S. Berendts, R. Uecker, W. C. Carter, Y. M. Chiang, *Adv. Energy Mater.* **2017**, *7*, 1701003.
[75] R. Garcia-Mendez, F. Mizuno, R. Zhang, T. S. Arthur, J. Sakamoto, *Electrochim. Acta* **2017**, *237*, 144.
[76] F. Han, A. S. Westover, J. Yue, X. Fan, F. Wang, M. Chi, D. N. Leonard, N. J. Dudney, H. Wang, C. Wang, *Nat. Energy* **2019**, *4*, 187.
[77] H. Morimoto, H. Yamashita, M. Tatsumisago, T. Minami, *J. Am. Chem. Soc.* **1999**, *82*, 1352.
[78] J. Auvergniot, A. Cassel, J.-B. Ledeuil, V. Viallet, V. Seznec, R. Dedryvère, *Chem. Mater.* **2017**, *29*, 3883.
[79] T. Hakari, M. Deguchi, K. Mitsuhara, T. Ohta, K. Saito, Y. Orikasa, Y. Uchimoto, Y. Kowada, A. Hayashi, M. Tatsumisago, *Chem. Mater.* **2017**, *29*, 4768.
[80] T. Hakari, M. Nagao, A. Hayashi, M. Tatsumisago, *J. Power Sources* **2015**, *293*, 721.
[81] R. Koerver, F. Walther, I. Aygün, J. Sann, C. Dietrich, W. G. Zeier, J. Janek, *J. Mater. Chem. A* **2017**, *5*, 22750.
[82] F. Han, T. Gao, Y. Zhu, K. J. Gaskell, C. Wang, *Adv. Mater.* **2015**, *27*, 3473.
[83] J. Haruyama, K. Sodeyama, L. Han, K. Takada, Y. Tateyama, *Chem. Mater.* **2014**, *26*, 4248.
[84] W. D. Richards, L. J. Miara, Y. Wang, J. C. Kim, G. Ceder, *Chem. Mater.* **2016**, *28*, 266.
[85] F. Han, Y. Zhu, X. He, Y. Mo, C. Wang, *Adv. Energy Mater.* **2016**, *6*, 1501590.
[86] A. Hayashi, H. Muramatsu, T. Ohtomo, S. Hama, M. Tatsumisago, *J. Mater. Chem. A* **2013**, *1*, 6320.
[87] S. Chen, D. Xie, G. Liu, J. P. Mwizerwa, Q. Zhang, Y. Zhao, X. Xu, X. Yao, *Energy Storage Mater.* **2018**, *14*, 58.
[88] G. Sahu, Z. Lin, J. Li, Z. Liu, N. Dudney, C. Liang, *Energy Environ. Sci.* **2014**, *7*, 1053.
[89] D. Y. Oh, D. H. Kim, S. H. Jung, J.-G. Han, N.-S. Choi, Y. S. Jung, *J. Mater. Chem. A* **2017**, *5*, 20771.
[90] A. Sakuda, K. Kuratani, M. Yamamoto, M. Takahashi, T. Takeuchi, H. Kobayashi, *J. Electrochem. Soc.* **2017**, *164*, A2474.
[91] T. Inada, K. Takada, A. Kajiyama, M. Kouguchi, H. Sasaki, S. Kondo, M. Watanabe, M. Murayama, R. Kanno, *Solid State Ionics* **2003**, *158*, 275.
[92] Y. J. Nam, S.-J. Cho, D. Y. Oh, J.-M. Lim, S. Y. Kim, J. H. Song, Y.-G. Lee, S.-Y. Lee, Y. S. Jung, *Nano Lett.* **2015**, *15*, 3317.
[93] L. Xu, S. Tang, Y. Cheng, K. Wang, J. Liang, C. Liu, Y.-C. Cao, F. Wei, L. Mai, *Joule* **2018**, *2*, 1991.
[94] J. M. Whiteley, S. Hafner, S. S. Han, S. C. Kim, K. H. Oh, S. H. Lee, *Adv. Energy Mater.* **2016**, *6*, 1600495.
[95] J. B. Goodenough, K. S. Park, *J. Am. Chem. Soc.* **2013**, *135*, 1167.
[96] J. B. Goodenough, Y. Kim, *Chem. Mater.* **2010**, *22*, 587.
[97] Q. Zhang, J. P. Mwizerwa, H. Wan, L. Cai, X. Xu, X. Yao, *J. Mater. Chem. A* **2017**, *5*, 23919.
[98] R. Xu, X. Wang, S. Zhang, Y. Xia, X. Xia, J. Wu, J. Tu, *J. Power Sources* **2018**, *374*, 107.
[99] F. Han, J. Yue, X. Fan, T. Gao, C. Luo, Z. Ma, L. Suo, C. Wang, *Nano Lett.* **2016**, *16*, 4521.
[100] H. M. Christen, G. Eres, *J. Phys.: Conden. Matter* **2008**, *20*, 264005.
[101] Y. Zhao, K. Zheng, X. Sun, *Joule* **2018**, *2*, 2853.
[102] K. Aso, A. Sakuda, A. Hayashi, M. Tatsumisago, *ACS Appl. Mater. Interfaces* **2013**, *5*, 686.
[103] A. Sakuda, A. Hayashi, T. Ohtomo, S. Hama, M. Tatsumisago, *Electrochem. Solid-State Lett.* **2010**, *13*, A73.
[104] A. Sakuda, A. Hayashi, T. Ohtomo, S. Hama, M. Tatsumisago, *J. Power Sources* **2011**, *196*, 6735.
[105] S. Yubuchi, Y. Ito, T. Matsuyama, A. Hayashi, M. Tatsumisago, *Solid State Ionics* **2016**, *285*, 79.
[106] B. R. Shin, Y. J. Nam, J. W. Kim, Y.-G. Lee, Y. S. Jung, *Sci. Rep.* **2014**, *4*, 5572.
[107] M. Nagao, A. Hayashi, M. Tatsumisago, *Electrochim. Acta* **2011**, *56*, 6055.
[108] R.-c. Xu, X.-h. Xia, X.-l. Wang, Y. Xia, J.-p. Tu, *J. Mater. Chem. A* **2017**, *5*, 2829.
[109] A. S. Arico, P. Bruce, B. Scrosati, J. M. Tarascon, W. Van Schalkwijk, *Nat. Mater.* **2005**, *4*, 366.
[110] F. Jiao, P. G. Bruce, *Adv. Mater.* **2007**, *19*, 657.
[111] P. Long, Q. Xu, G. Peng, X. Yao, X. Xu, *ChemElectroChem* **2016**, *3*, 764.
[112] Q. Zhang, G. Peng, J. P. Mwizerwa, H. Wan, L. Cai, X. Xu, X. Yao, *J. Mater. Chem. A* **2018**, *6*, 12098.
[113] E. Umeshbabu, B. Zheng, Y. Yang, *Electrochem. Energy Rev.* **2019**, *2*, 199.
[114] Z. Lin, C. Liang, *J. Mater. Chem. A* **2015**, *3*, 936.
[115] A. Hayashi, T. Ohtomo, F. Mizuno, K. Tadanaga, M. Tatsumisago, *Electrochem. Commun.* **2003**, *5*, 701.
[116] T. Kobayashi, Y. Imade, D. Shishihara, K. Homma, M. Nagao, R. Watanabe, T. Yokoi, A. Yamada, R. Kanno, T. Tatsumi, *J. Power Sources* **2008**, *182*, 621.
[117] M. Nagao, Y. Imade, H. Narisawa, T. Kobayashi, R. Watanabe, T. Yokoi, T. Tatsumi, R. Kanno, *J. Power Sources* **2013**, *222*, 237.
[118] A. Sakuda, Y. Sato, A. Hayashi, M. Tatsumisago, *Energy Technol.* **2019**, *7*, 1900077.
[119] H. Nagata, Y. Chikusa, *J. Power Sources* **2014**, *264*, 206.

[120] X. Yao, N. Huang, F. Han, Q. Zhang, H. Wan, J. P. Mwizerwa, C. Wang, X. Xu, *Adv. Energy Mater.* **2017**, *7*, 1602923.
[121] Q. Zhang, N. Huang, Z. Huang, L. Cai, J. Wu, X. Yao, *J. Energy Chem.* **2020**, *40*, 151.
[122] Y. Zhang, Y. Sun, L. Peng, J. Yang, H. Jia, Z. Zhang, B. Shan, J. Xie, *Energy Storage Mater.* **2019**, *21*, 287.
[123] E. Kazyak, K.-H. Chen, A. L. Davis, S. Yu, A. J. Sanchez, J. Lasso, A. R. Bielinski, T. Thompson, J. Sakamoto, D. J. Siegel, N. P. Dasgupta, *J. Mater. Chem. A* **2018**, *6*, 19425.
[124] H. Yan, H. Wang, D. Wang, X. Li, Z. Gong, Y. Yang, *Nano Lett.* **2019**, *19*, 3280.
[125] A. Hayashi, R. Ohtsubo, T. Ohtomo, F. Mizuno, M. Tatsumisago, *J. Power Sources* **2008**, *183*, 422.
[126] M. Nagao, A. Hayashi, M. Tatsumisago, *J. Mater. Chem.* **2012**, *22*, 10015.
[127] T. Hakari, A. Hayashi, M. Tatsumisago, *Adv. Sustainable Syst.* **2017**, *1*, 1700017.
[128] Z. Lin, Z. Liu, N. J. Dudney, C. Liang, *ACS Nano* **2013**, *7*, 2829.
[129] Z. Lin, Z. Liu, W. Fu, N. J. Dudney, C. Liang, *Angew. Chem., Int. Ed.* **2013**, *52*, 7460.
[130] B.-C. Kim, K. Takada, N. Ohta, Y. Seino, L. Zhang, H. Wada, T. Sasaki, *Solid State Ionics* **2005**, *176*, 2383.
[131] C. Xing, D. Zhang, K. Cao, S. Zhao, X. Wang, H. Qin, J. Liu, Y. Jiang, L. Meng, *J. Mater. Chem. A* **2015**, *3*, 8742.
[132] Q. Zhang, X. Yao, J. P. Mwizerwa, N. Huang, H. Wan, Z. Huang, X. Xu, *Solid State Ionics* **2018**, *318*, 60.
[133] K. Aso, H. Kitaura, A. Hayashi, M. Tatsumisago, *J. Mater. Chem.* **2011**, *21*, 2987.
[134] Y. Nishio, H. Kitaura, A. Hayashi, M. Tatsumisago, *J. Power Sources* **2009**, *189*, 629.
[135] K. Aso, A. Hayashi, M. Tatsumisago, *Electrochim. Acta* **2012**, *83*, 448.
[136] E. D. Grayfer, E. M. Pazhetnov, M. N. Kozlova, S. B. Artemkina, V. E. Fedorov, *ChemSusChem* **2017**, *10*, 4805.
[137] T. A. Yersak, H. A. Macpherson, S. C. Kim, V.-D. Le, C. S. Kang, S.-B. Son, Y.-H. Kim, J. E. Trevey, K. H. Oh, C. Stoldt, S.-H. Lee, *Adv. Energy Mater.* **2013**, *3*, 120.
[138] H. Wan, G. Liu, Y. Li, W. Weng, J. P. Mwizerwa, Z. Tian, L. Chen, X. Yao, *ACS Nano* **2019**, *13*, 9551.
[139] Y. J. Zhu, X. L. Fan, L. M. Suo, C. Luo, T. Gao, C. S. Wang, *ACS Nano* **2016**, *10*, 1529.
[140] T. Matsuyama, A. Hayashi, T. Ozaki, S. Mori, M. Tatsumisago, *J. Mater. Chem. A* **2015**, *3*, 14142.
[141] T. Matsuyama, M. Deguchi, K. Mitsuhara, T. Ohta, T. Mori, Y. Orikasa, Y. Uchimoto, Y. Kowada, A. Hayashi, M. Tatsumisago, *J. Power Sources* **2016**, *313*, 104.
[142] Q. Zhang, Z. Ding, G. Liu, H. Wan, J. P. Mwizerwa, J. Wu, X. Yao, *Energy Storage Mater.* **2019**, *23*, 168.
[143] Q. Zhang, H. Wan, G. Liu, Z. Ding, J. P. Mwizerwa, X. Yao, *Nano Energy* **2019**, *57*, 771.
[144] A. Sakuda, K. Ohara, K. Fukuda, K. Nakanishi, T. Kawaguchi, H. Arai, Y. Uchimoto, T. Ohta, E. Matsubara, Z. Ogumi, *J. Am. Chem. Soc.* **2017**, *139*, 8796.
[145] U. Ulissi, S. Ito, S. M. Hosseini, A. Varzi, Y. Aihara, S. Passerini, *Adv. Energy Mater.* **2018**, *8*, 1801462.
[146] N. Tanibata, H. Tsukasaki, M. Deguchi, S. Mori, A. Hayashi, M. Tatsumisago, *J. Mater. Chem. A* **2017**, *5*, 11224.
[147] P. G. Bruce, S. A. Freunberger, L. J. Hardwick, J.-M. Tarascon, *Nat. Mater.* **2012**, *11*, 19.
[148] J. W. Choi, D. Aurbach, *Nat. Rev. Mater.* **2016**, *1*, 16013.
[149] X.-B. Cheng, R. Zhang, C.-Z. Zhao, Q. Zhang, *Chem. Rev.* **2017**, *117*, 10403.
[150] X. B. Cheng, R. Zhang, C. Z. Zhao, F. Wei, J. G. Zhang, Q. Zhang, *Adv. Sci.* **2016**, *3*, 1500213.
[151] S. Wenzel, T. Leichtweiss, D. Krüger, J. Sann, J. Janek, *Solid State Ionics* **2015**, *278*, 98.
[152] P. Hartmann, T. Leichtweiss, M. R. Busche, M. Schneider, M. Reich, J. Sann, P. Adelhelm, J. Janek, *J. Phys. Chem. C* **2013**, *117*, 21064.
[153] S. J. Visco, V. Y. Nimon, A. Petrov, K. Pridatko, N. Goncharenko, E. Nimon, L. De Jonghe, Y. M. Volfkovich, D. A. Bograchev, *J. Solid State Electrochem.* **2014**, *18*, 1443.
[154] H. Wang, D. Im, D. Lee, M. Matsui, Y. Takeda, O. Yamamoto, N. Imanishi, *J. Electrochem. Soc.* **2013**, *160*, A728.
[155] J. Reinacher, S. Berendts, J. Janek, *Solid State Ionics* **2014**, *258*, 1.
[156] Y. Zhu, X. He, Y. Mo, *ACS Appl. Mater. Interfaces* **2015**, *7*, 23685.
[157] L. E. Camacho-Forero, P. B. Balbuena, *J. Power Sources* **2018**, *396*, 782.
[158] S. Wenzel, S. Randau, T. Leichtweiß, D. A. Weber, J. Sann, W. G. Zeier, J. r. Janek, *Chem. Mater.* **2016**, *28*, 2400.
[159] S. Wenzel, S. J. Sedlmaier, C. Dietrich, W. G. Zeier, J. Janek, *Solid State Ionics* **2018**, *318*, 102.
[160] T. Cheng, B. V. Merinov, S. Morozov, W. A. Goddard III, *ACS Energy Lett.* **2017**, *2*, 1454.
[161] K. N. Wood, K. X. Steirer, S. E. Hafner, C. Ban, S. Santhanagopalan, S.-H. Lee, G. Teeter, *Nat. Commun.* **2018**, *9*, 2490.
[162] Y. Shen, Y. Zhang, S. Han, J. Wang, Z. Peng, L. Chen, *Joule* **2018**, *2*, 1674.
[163] C. Monroe, J. Newman, *J. Electrochem. Soc.* **2005**, *152*, A396.
[164] Y. Takeda, O. Yamamoto, N. Imanishi, *Electrochemistry* **2016**, *84*, 210.
[165] Y. Ren, Y. Shen, Y. Lin, C.-W. Nan, *Electrochem. Commun.* **2015**, *57*, 27.
[166] P. Barai, K. Higa, V. Srinivasan, *J. Electrochem. Soc.* **2017**, *164*, A180.
[167] C. Brissot, M. Rosso, J. N. Chazalviel, S. Lascaud, *J. Power Sources* **1999**, *81–82*, 925.
[168] Z. Zhang, L. Zhang, Y. Liu, H. Wang, C. Yu, H. Zeng, L. m. Wang, B. Xu, *ChemSusChem* **2018**, *11*, 3774.
[169] S. Wang, H. Xu, W. Li, A. Dolocan, A. Manthiram, *J. Am. Chem. Soc.* **2018**, *140*, 250.
[170] X. Wang, R. Xiao, H. Li, L. Chen, *Phys. Chem. Chem. Phys.* **2016**, *18*, 21269.
[171] Z. Zhang, L. Zhang, X. Yan, H. Wang, Y. Liu, C. Yu, X. Cao, L. van Eijck, B. Wen, *J. Power Sources* **2019**, *410–411*, 162.
[172] Y. Sun, K. Suzuki, K. Hara, S. Hori, T.-a. Yano, M. Hara, M. Hirayama, R. Kanno, *J. Power Sources* **2016**, *324*, 798.
[173] D. Xie, S. Chen, Z. Zhang, J. Ren, L. Yao, L. Wu, X. Yao, X. Xu, *J. Power Sources* **2018**, *389*, 140.
[174] G. Liu, D. Xie, X. Wang, X. Yao, S. Chen, R. Xiao, H. Li, X. Xu, *Energy Storage Mater.* **2019**, *17*, 266.
[175] M. Suyama, A. Kato, A. Sakuda, A. Hayashi, M. Tatsumisago, *Electrochim. Acta* **2018**, *286*, 158.
[176] B. Huang, X. Yao, Z. Huang, Y. Guan, Y. Jin, X. Xu, *J. Power Sources* **2015**, *284*, 206.
[177] Y. Sun, W. Yan, L. An, B. Wu, K. Zhong, R. Yang, *Solid State Ionics* **2017**, *301*, 59.
[178] S. H. Jung, K. Oh, Y. J. Nam, D. Y. Oh, P. Brüner, K. Kang, Y. S. Jung, *Chem. Mater.* **2018**, *30*, 8190.
[179] R. Xu, F. Han, X. Ji, X. Fan, J. Tu, C. Wang, *Nano Energy* **2018**, *53*, 958.
[180] M. Ogawa, R. Kanda, K. Yoshida, T. Uemura, K. Harada, *J. Power Sources* **2012**, *205*, 487.
[181] A. Kato, A. Hayashi, M. Tatsumisago, *J. Power Sources* **2016**, *309*, 27.
[182] A. Kato, H. Kowada, M. Deguchi, C. Hotehama, A. Hayashi, M. Tatsumisago, *Solid State Ionics* **2018**, *322*, 1.
[183] M. Nagao, A. Hayashi, M. Tatsumisago, *Electrochem. Commun.* **2012**, *22*, 177.
[184] Z. Zhang, S. Chen, J. Yang, J. Wang, L. Yao, X. Yao, P. Cui, X. Xu, *ACS Appl. Mater. Interfaces* **2018**, *10*, 2556.
[185] Y. Lu, Z. Tu, L. A. Archer, *Nat. Mater.* **2014**, *13*, 961.

[186] X. Fan, L. Chen, X. Ji, T. Deng, S. Hou, J. Chen, J. Zheng, F. Wang, J. Jiang, K. Xu, *Chem* **2018**, *4*, 174.
[187] X. Fan, X. Ji, F. Han, J. Yue, J. Chen, L. Chen, T. Deng, J. Jiang, C. Wang, *Sci. Adv.* **2018**, *4*, eaau9245.
[188] Y. Zhang, R. Chen, S. Wang, T. Liu, B. Xu, X. Zhang, X. Wang, Y. Shen, Y.-H. Lin, M. Li, *Energy Storage Mater.* **2020**, *25*, 145.
[189] C. Wang, K. R. Adair, J. Liang, X. Li, Y. Sun, X. Li, J. Wang, Q. Sun, F. Zhao, X. Lin, R. Li, H. Huang, L. Zhang, R. Yang, S. Lu, X. Sun, *Adv. Funct. Mater.* **2019**, *29*, 1900392.
[190] J. Dai, C. Yang, C. Wang, G. Pastel, L. Hu, *Adv. Mater.* **2018**, *30*, 1802068.
[191] A. Kızılaslan, H. Akbulut, *ChemPlusChem* **2019**, *84*, 183.
[192] F. Zheng, M. Kotobuki, S. Song, M. O. Lai, L. Lu, *J. Power Sources* **2018**, *389*, 198.
[193] K. Takada, N. Aotani, K. Iwamoto, S. Kondo, *Solid State Ionics* **1996**, *86–88*, 877.
[194] F. Sun, K. Dong, M. Osenberg, A. Hilger, S. Risse, Y. Lu, P. H. Kamm, M. Klaus, H. Markötter, F. García-Moreno, T. Arlt, I. Manke, *J. Mater. Chem. A* **2018**, *6*, 22489.
[195] R. Kanno, M. Murayama, T. Inada, T. Kobayashi, K. Sakamoto, N. Sonoyama, A. Yamada, S. Kondo, *Electrochem. Solid-State Lett.* **2004**, *7*, A455.
[196] T. Kobayashi, A. Yamada, R. Kanno, *Electrochim. Acta* **2008**, *53*, 5045.
[197] M. Sakuma, K. Suzuki, M. Hirayama, R. Kanno, *Solid State Ionics* **2016**, *285*, 101.
[198] Y. Liu, P. He, H. Zhou, *Adv. Energy Mater.* **2018**, *8*, 1701602.
[199] Y.-C. Jung, S.-M. Lee, J.-H. Choi, S. S. Jang, D.-W. Kim, *J. Electrochem. Soc.* **2015**, *162*, A704.
[200] L. Cai, Q. Zhang, J. P. Mwizerwa, H. Wan, X. Yang, X. Xu, X. Yao, *ACS Appl. Mater. Interfaces* **2018**, *10*, 10053.
[201] H. Wan, G. Peng, X. Yao, J. Yang, P. Cui, X. Xu, *Energy Storage Mater.* **2016**, *4*, 59.
[202] J. H. Cho, G. B. Kim, H. S. Lim, M. L. Liu, *J. Electrochem. Soc.* **1998**, *145*, 1949.
[203] Y. R. Zhao, C. Wu, G. Peng, X. T. Chen, X. Y. Yao, Y. Bai, F. Wu, S. J. Chen, X. X. Xu, *J. Power Sources* **2016**, *301*, 47.
[204] S. Chen, J. Wang, Z. Zhang, L. Wu, L. Yao, Z. Wei, Y. Deng, D. Xie, X. Yao, X. Xu, *J. Power Sources* **2018**, *387*, 72.
[205] A. Hayashi, T. Harayama, F. Mizuno, M. Tatsumisago, *J. Power Sources* **2006**, *163*, 289.
[206] I. Villaluenga, K. H. Wujcik, W. Tong, D. Devaux, D. H. Wong, J. M. DeSimone, N. P. Balsara, *Proc. Natl. Acad. Sci. USA* **2016**, *113*, 52.
[207] J. M. Whiteley, P. Taynton, W. Zhang, S. H. Lee, *Adv. Mater.* **2015**, *27*, 6922.
[208] Z. D. Hood, H. Wang, A. S. Pandian, R. Peng, K. D. Gilroy, M. Chi, C. Liang, Y. Xia, *Adv. Energy Mater.* **2018**, *8*, 1800014.
[209] L.-P. Hou, H. Yuan, C.-Z. Zhao, L. Xu, G.-L. Zhu, H.-X. Nan, X.-B. Cheng, Q.-B. Liu, C.-X. He, J.-Q. Huang, *Energy Storage Mater.* **2020**, *25*, 436.
[210] S. Ohno, R. Koerver, G. Dewald, C. Rosenbach, P. Titscher, D. Steckermeier, A. Kwade, J. r. Janek, W. G. Zeier, *Chem. Mater.* **2019**, *31*, 2930.
[211] P. Bonnick, K. Niitani, M. Nose, K. Suto, T. S. Arthur, J. Muldoon, *J. Mater. Chem. A* **2019**, *7*, 24173.
[212] C. Yu, L. van Eijck, S. Ganapathy, M. Wagemaker, *Electrochim. Acta* **2016**, *215*, 93.
[213] J. E. Trevey, J. R. Gilsdorf, C. R. Stoldt, S.-H. Lee, P. Liu, *J. Electrochem. Soc.* **2012**, *159*, A1019.
[214] T. Yamada, S. Ito, R. Omoda, T. Watanabe, Y. Aihara, M. Agostini, U. Ulissi, J. Hassoun, B. Scrosati, *J. Electrochem. Soc.* **2015**, *162*, A646.
[215] K. Suzuki, D. Kato, K. Hara, T.-a. Yano, M. Hirayama, M. Hara, R. Kanno, *Electrochemistry* **2018**, *86*, 1.
[216] K. Suzuki, N. Mashimo, Y. Ikeda, T. Yokoi, M. Hirayama, R. Kanno, *ACS Appl. Mater. Interfaces* **2018**, *1*, 2373.
[217] M. Agostini, Y. Aihara, T. Yamada, B. Scrosati, J. Hassoun, *Solid State Ionics* **2013**, *244*, 48.
[218] M. Chen, S. Adams, *J. Solid State Electrochem.* **2015**, *19*, 697.
[219] S. Kinoshita, K. Okuda, N. Machida, M. Naito, T. Sigematsu, *Solid State Ionics* **2014**, *256*, 97.
[220] K. Suzuki, D. Kato, K. Hara, T.-a. Yano, M. Hirayama, M. Hara, R. Kanno, *Electrochim. Acta* **2017**, *258*, 110.
[221] S. Kinoshita, K. Okuda, N. Machida, T. Shigematsu, *J. Power Sources* **2014**, *269*, 727.
[222] C. Yu, S. Ganapathy, E. R. van Eck, L. van Eijck, S. Basak, Y. Liu, L. Zhang, H. W. Zandbergen, M. Wagemaker, *J. Mater. Chem. A* **2017**, *5*, 21178.
[223] R. Xu, J. Yue, S. Liu, J. Tu, F. Han, P. Liu, C. Wang, *ACS Energy Lett.* **2019**, *4*, 1073.
[224] M. Nagao, A. Hayashi, M. Tatsumisago, T. Ichinose, T. Ozaki, Y. Togawa, S. Mori, *J. Power Sources* **2015**, *274*, 471.